

# An Experimental Study of Liquid Compositions in Equilibrium with Plagioclase + Spinel Lherzolite at Low Pressures (0.75 GPa)

FRANÇOISE CHALOT-PRAT<sup>1\*</sup>, TREVOR J. FALLOON<sup>2</sup>,  
DAVID H. GREEN<sup>2,3</sup> AND WILLIAM O. HIBBERSON<sup>3</sup>

<sup>1</sup>CRPG-CNRS/NANCY UNIVERSITÉ, 15 RUE NOTRE DAME DES PAUVRES, BP20, 54501 VANDOEUVRE LES NANCY, FRANCE

<sup>2</sup>ARC CENTRE OF EXCELLENCE IN ORE DEPOSITS AND SCHOOL OF EARTH SCIENCES, UNIVERSITY OF TASMANIA, PRIVATE BAG 79, HOBART, TASMANIA 7001, AUSTRALIA

<sup>3</sup>RESEARCH SCHOOL OF EARTH SCIENCES, THE AUSTRALIAN NATIONAL UNIVERSITY, CANBERRA, ACT 0200, AUSTRALIA

RECEIVED OCTOBER 19, 2009; ACCEPTED SEPTEMBER 8, 2010

*Models of formation of basaltic crust at mid-ocean ridges by adiabatic upwelling of fertile mantle lherzolite require knowledge of phase relations and phase compositions during melting at appropriate pressures. Spinel + plagioclase lherzolites are found among peridotite samples from the ocean floor and ophiolitic exposures. At low pressure (<1.2 GPa) the five-phase assemblage (olivine + orthopyroxene + clinopyroxene + plagioclase + spinel) is present at the anhydrous lherzolite solidus. New experimental data on mineral and melt compositions, at 0.75 GPa and 1140–1260°C in the (Cr + Na + Fe + Ca + Mg + Al + Si) system, demonstrate smooth covariant relationships between oxides for melt compositions and in partition relationships both between mineral pairs and between minerals and melts. Molecular normative projections demonstrate that liquids on the five-phase + liquid cotectic occupy a narrow compositional range. Of the mineral solid solutions that control the liquid composition, the [Ca/(Ca + Na)] or anorthite/albite content of the plagioclase is dominant and liquids vary from silica undersaturated and nepheline-normative at the sodic (oligoclase) end to orthopyroxene and quartz-normative at the calcic (anorthite) end of the cotectic. Spinel (Cr–Al) solid solution has limited variation on the five-phase + liquid cotectic. It is very Cr-rich at the sodic end and has limited compositional variation from ~50 to 20 in Cr/(Cr + Al) at the anorthitic end. With fixed plagioclase composition on the cotectic, melt compositions show small compositional shifts with Fe–Mg (at Mg# between*

*85 and 95) and with Cr/(Cr + Al). The compositional vectors are consistent with effects observed in the end-member simple systems (FCMAS) and (CrCMAS). In comparing liquids at the anorthite end of the five-phase + liquid cotectic with those on the Cr-free CMAS four-phase + liquid cotectic at 0.75 GPa, it is evident that the presence of Al-rich Cr–Al spinel shifts liquid compositions to more silica-rich and silica-oversaturated composition. These experimentally defined melt compositions in equilibrium with plagioclase + spinel lherzolite are unlike quenched glasses from mid-ocean ridge settings. The data do not support models of mantle upwelling at low potential temperature (1280°C) that produces low melt fractions at low pressures, leaving residual plagioclase + spinel lherzolite. The detailed mineral compositional data at the solidus provide a template for comparison with natural plagioclase + spinel lherzolites refertilized by porous reactive flow.*

KEY WORDS: experiments; lherzolite; low pressure; MORB; plagioclase; spinel

## INTRODUCTION

This study is a contribution towards understanding the melting behaviour of the Earth's upper mantle, focused on liquid compositions formed at low pressure (0.75 GPa), at

\*Corresponding author. E-mail: chalot@crpg.cnrs-nancy.fr

near-solidus temperatures, from plagioclase + spinel lherzolites. In widely used models of melt extraction and lithosphere formation at mid-ocean ridges (MORs), asthenospheric mantle of lherzolite composition [Primitive Modern Mantle (PMM) or MOR Pyrolite] is conceived as passively upwelling in response to lithospheric plate stretching and rupture (McKenzie & Bickle, 1988). If the broad-scale upwelling approaches adiabatic conditions, then the upwelling lherzolite will cross the anhydrous solidus of (C + H)-free lherzolite or pass from the incipient melting regime [small liquid fraction controlled by (C + H) concentration, i.e.  $\text{CO}_3^{2-}$  and  $\text{OH}^-$  solubility] into the major melting regime of lherzolite + (C, H, O) (Green & Falloon, 1998). The experimentally determined solidi of volatile-free lherzolite compositions exhibit a change in slope (increase of  $dT/dP$ ) at pressures from 0.7 to 1.3 GPa where plagioclase disappears from the solidus mineral assemblage (Green & Falloon, 1998). The role of this 'cusp' on the solidus as a controlling feature in localizing mantle melting has been debated (Presnall & Hoover, 1987; Asimow *et al.*, 2001; Presnall *et al.*, 2002) and used in modelling of upwelling to argue for relatively low mantle potential temperatures beneath mid-ocean ridges (McKenzie & Bickle, 1988; Presnall *et al.*, 2002).

Estimates of upper mantle composition concur at lherzolite with 3–4% CaO and 3–4%  $\text{Al}_2\text{O}_3$  (Hart & Zindler, 1986; Green & Falloon, 1998). Using natural or normative mineral compositions and mixing calculations, it can be shown that such compositions have ~10% modal plagioclase at low-pressure and high-temperature conditions. Extraction of <10–12% melt fractions, whether by batch or fractional melting processes, will leave depleted lherzolite compositions including residual plagioclase at low pressure. Some geophysical models of mid-ocean ridge upwelling relate ocean crust thickness to mantle potential temperature and suggest average melt depletion by 5–7% melting in the mantle column beneath normal oceanic crust of <10 km thickness (McKenzie & Bickle, 1988). If fertile lherzolite compositions are preserved to shallow depths in upwelling mantle, particularly at mantle potential temperatures of <1300°C, then the residual lherzolite mineralogy from single-stage melting at depths <30 km will include plagioclase.

Detailed studies of recent and fossil spreading ridge settings, including field, petrographical and geochemical observations, have led some workers (Stakes *et al.*, 1984; Chalot-Prat, 2005) to infer a shallow depth of melt segregation from upwelling residual mantle. Sets of small volcanoes formed at the ridge axis show eruption of both parental magmas, interpreted as partial melts of a depleted asthenospheric mantle, and differentiates of such magmas. Rapid alternation between the two magma types suggests that each volcanic centre is related to a frequently fed small reservoir close to a rather

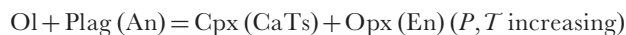
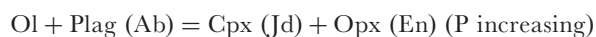
shallow mantle source. In addition, the inference of close coupling between mechanical extension characteristics (spreading rates, lithospheric mantle exhumation and related distribution of magma conduits at the axial zone) and eruptive process (magma emplacement and volcano formation at the axial zone) also suggests shallow rather than deep levels of mantle upwelling and magma separation.

Natural occurrences of plagioclase lherzolite have been reviewed by Piccardo *et al.* (2007, and references therein), Müntener *et al.* (2010) and Borghini *et al.* (2010). These studies have advocated the production of plagioclase lherzolite in the uppermost lithosphere by invasive percolation of basaltic melt into pre-existing high-temperature residual peridotite. Piccardo *et al.* (2007) and Müntener *et al.* (2010) described examples of melt–rock reaction or 'refertilization' and considered that magma storage in the uppermost mantle in this way is a major process at magma-poor rifted margins and at magma-starved mid-ocean ridge segments. Borghini *et al.* (2010) emphasized two origins for natural plagioclase lherzolites; that is, either by metamorphic recrystallization during decompression of spinel lherzolite at low pressure and high temperature, or by basaltic melt impregnation into high-temperature residual peridotite at low pressure and consequent reaction and crystallization. In these interpretations, the role of melting of plagioclase lherzolite has relevance to understanding the chemical evolution of a basaltic melt permeating and reacting with lherzolite that includes the five-phase mineralogy [olivine (Ol) + enstatite (Opx) + diopside (Cpx) + plagioclase (Plag) + spinel (Sp)]. Van Den Bleeken *et al.* (2010) have recently investigated the reactive porous flow concept by experimentally passing basaltic melts through residual spinel lherzolite layers at 0.8 GPa. In choosing a pressure of 0.8 GPa for their study, those researchers aimed to simulate conditions within the transition zone or thermal boundary layer between near-adiabatic upwelling mantle during lithospheric thinning and the thermal conductive regime of the thinned lithosphere. The experiments demonstrated melt–residue interaction and chemical evolution of both lherzolite and melt compositions, commonly with mineral zoning, except at the highest temperatures and melt fractions. A few of their runs contained the five-phase plagioclase + spinel lherzolite assemblage and demonstrated a role for this mineral assemblage in controlling the composition of melts at near-solidus conditions. The present investigation complements the work of Van Den Bleeken *et al.* (2010) by determining the compositions of equilibrium liquids at the  $P,T$  conditions of interest.

A further motivation for this study is a contribution towards the growing experimental database on coexisting melt and mineral compositions at high pressures.

These data are the necessary inputs and/or tests for the calculation of numerical or thermodynamic models of melting at various pressures (Asimow *et al.*, 2001; Ghiorso *et al.*, 2002). By designing an experimental study that at a fixed pressure provides the compositions of the melt and all coexisting phases (all of which are solid solutions) in equilibrium at appropriate temperatures, it is possible to evaluate and if necessary modify such melting models.

With these diverse objectives in mind, we have chosen to determine liquid (Liq) compositions in equilibrium, at a pressure of 0.75 GPa, with five residual phases (Ol + Opx + Cpx + Plag + Sp). Of equal importance to the liquid composition are the compositions of the solid phases, all of them solid solutions of varying complexity. A relatively constant Mg# [100Mg/(Mg + Fe)] in pyroxenes and olivine has been maintained, with olivine between Mg<sub>89</sub> and Mg<sub>95</sub>. Plagioclase composition was varied from An<sub>0</sub> to An<sub>100</sub> [An = Ca/(Ca + Na) (mol) of plagioclase]. Sufficient Cr<sub>2</sub>O<sub>3</sub> was added to compositions to maintain the presence of a Cr–Al spinel. Spinel and pyroxene vary in composition in response to solid solution of components such as: NaCrSi<sub>2</sub>O<sub>6</sub>, CaCrAlSiO<sub>6</sub> and CaAl<sub>2</sub>SiO<sub>6</sub> in diopside; MgCrAlSiO<sub>6</sub> and MgAl<sub>2</sub>SiO<sub>6</sub> in enstatite; Fe<sub>3</sub>O<sub>4</sub>, (MgFe)Cr<sub>2</sub>O<sub>4</sub> and (MgFe)Al<sub>2</sub>O<sub>4</sub> in spinel. These solid solution components are also participants in *P,T*-dependent reactions involving plagioclase and olivine, so that chemical equilibria may be devised to relate mineral compositions and *P,T* conditions:



(i.e. the pyroxene miscibility gap).

By the experimental determination of mineral and liquid compositions on the six-phase saturation surface, as functions of pressure and temperature, a dataset is obtained from which numerical melting models in the plagioclase + spinel lherzolite field can be constructed. In addition, the melt and mineral composition data at known pressure and temperature provide a basis for interpretation of natural plagioclase + spinel lherzolites and mantle-derived basaltic liquids. These comparisons and interpretations apply to the Ca-rich part of the experimental series. The extension beyond the range of natural lherzolite compositions into Na-rich compositions aids the extraction of data for different solid solutions.

## EXPERIMENTAL METHODS

### Experimental assemblies

All experiments used either 1.27 cm or 1.6 cm diameter, end-loaded piston-cylinder apparatus at the Research School of Earth Sciences (The Australian National University). Standard NaCl–Pyrex assemblies had graphite heaters and type B Pt–Rh thermocouples. Because of the NaCl–Pyrex assemblies and long run times, no pressure corrections were applied and sample pressure was equated with measured load pressure. Two types of capsule were used successfully (Fig. 1a and b). Initially we used olivine capsules sealed within platinum to avoid iron loss and maintain olivine saturation (Fig. 1a). However, some anomalous results and observation of large cavities within the olivine capsule suggested that the olivine container was sufficiently strong to maintain a low internal pressure in some experiments. Data from three experiments in olivine capsules are included in our final selection. In these experiments, no temperature correction is applied as both thermocouple and the small sample capsule are within the ‘hotspot’ of the sample assembly.

To avoid Fe-loss problems we used large Au<sub>25</sub>Pd<sub>75</sub> containers containing three small-diameter Au<sub>25</sub>Pd<sub>75</sub> capsules, each with a different mix (Fig. 1b). The inner capsules were surrounded by an Fe-enriched hydrous basanite melt that was close to or above its liquidus and in which the liquidus phases were olivine and/or magnetite. The iron-rich external melt effectively ‘saturated’ the Fe content of the inner capsule walls and ensured that little or no Fe loss or gain was experienced by the charge within the inner capsules, maintaining the Mg# of olivine in the inner capsules very close to the desired value. Temperatures were controlled to ±1°C of the set point. Prior calibration of the sample assembly using multiple thermocouples gave a temperature correction of +20°C between thermocouple and sample.

An advantage of the three-capsule method is that we have three different bulk compositions at exactly the same *P,T*. Differences in phase assemblages and glass or mineral compositions between the three bulk compositions must reflect compositional control on phase assemblages and not differences in *P,T*. The use of a thick-walled AuPd outer capsule and the volume (~50 mg) of basanite melt around the three capsules acts to homogenize temperature throughout the 1–1.5 mm length of the charge. The absence of a significant thermocouple gradient in the sample is also supported by the homogeneity of the liquid and phase compositions over the length of the charge. A disadvantage of the three-capsule method is that the thermocouple is at greater separation from the sample than in normal single-capsule set-ups. Although calibration runs on thermal gradients within the pressure cell allow us to make a correction of +20°C, we do not consider run temperature measurement to be better than ±20°C.

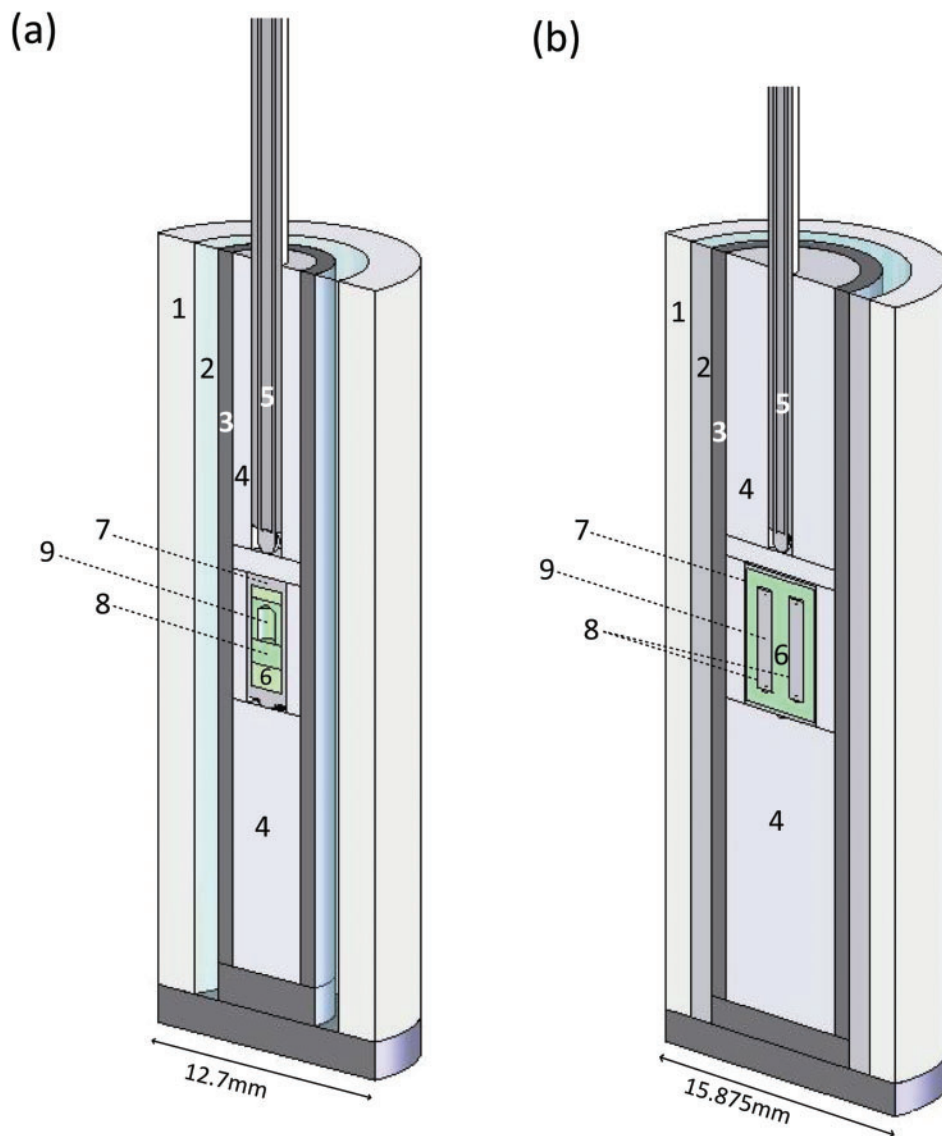


**Fig. 1.** High-pressure cell assemblies used in experiments at 0.75 GPa. (a) Single-capsule assembly using olivine container sealed in platinum tube; 1, 12.7 mm NaCl sleeve; 2, Pyrex; 3, graphite heater; 4, MgO; 5, type 'B' thermocouple in two-bore mullite tube; 6, olivine powder; 7, 2.3 mm Pt capsule; 8, 1.8 mm olivine capsule; 9, sample. (b) Three AuPd capsules within 5 mm diameter AuPd tube containing olivine basanite + fayalite mixture; 1, 15.875 mm NaCl sleeve; 2–6 and 9, same as in (a); 7, AuPd 5 mm capsule; 8, two of three AuPd 1.6 mm capsules.

Experimental charges were mounted within their olivine or AuPd capsules, sectioned longitudinally and polished for examination by reflected light and scanning electron microscopy (JEOL 6400 SEM). Typical run products are illustrated in Fig. 2.

### Analytical methods

Phase compositions were determined by energy dispersive X-ray analysis (EDS) using a JEOL 6400 SEM, accelerating voltage of 15 kV, specimen current of 1 nA, and analysis time of 100 s. A recent comparison of data obtained on the

same instrument and with the same analytical conditions and calibrations with data obtained by wavelength-dispersive spectrometry using an electron microprobe (Spandler *et al.*, 2010) demonstrated the satisfactory quality of the methods. Selection of acceptable analyses was based on totals from 97.5 to 102% and, more importantly, on satisfactory stoichiometry of olivine, plagioclase, pyroxenes or spinel.

The very small size of spinel in some experiments yielded analyses with >1% SiO<sub>2</sub> and corresponding anomalous concentrations of CaO and Na<sub>2</sub>O. Such spinels were

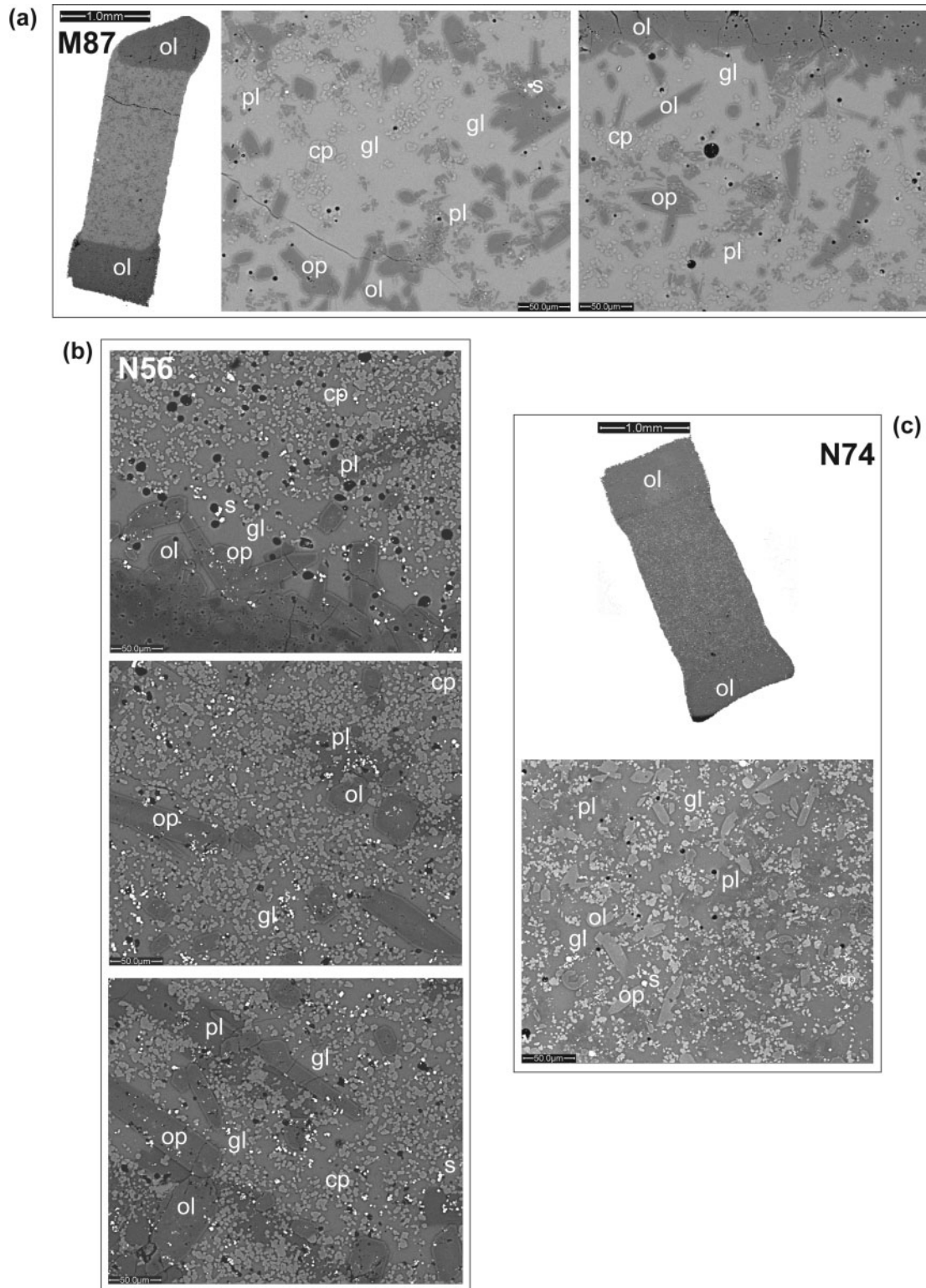


**Fig. 2.** Scanning electron microscope images of experimental charges illustrating the 'sandwich' of sample between olivine layers and glass-rich character of sample to avoid quench modification of glass composition (melt) by quench outgrowths on pyroxenes particularly. Phases labeled: ol, olivine; op, orthopyroxene; cp, clinopyroxene; pl, plagioclase; s, spinel; gl, glass. Sample numbers: (a) M87; (b) N56; (c) N74.

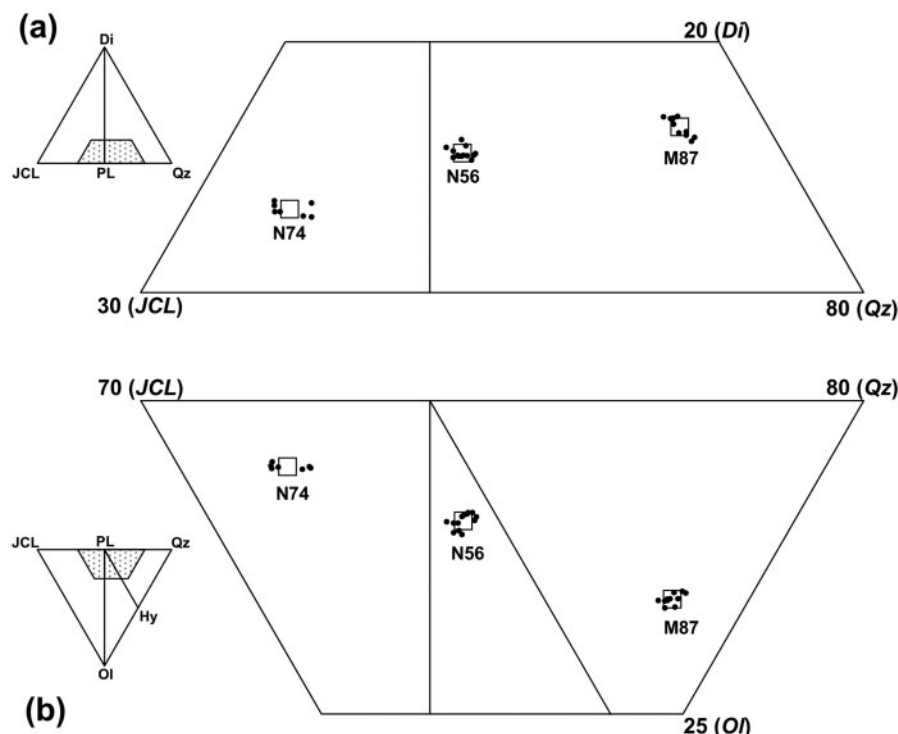


**Fig. 3.** Single analyses (dots) and calculated average composition (squares) of glasses from the experiments illustrated in Fig. 2 projected into a part of the normative tetrahedron (see insets). (a) is projected from Olivine to the face Diopside, Jadeite + Ca Tschermak's silicate + Leucite (JCL), Quartz. (b) is projected from Olivine to the face Olivine, Jadeite + Ca Tschermak's silicate + Leucite, Quartz.

included in glass or more rarely in plagioclase or orthopyroxene. The analysis was then corrected by subtraction of the appropriate phase composition to reduce  $\text{SiO}_2$  and CaO to zero. These corrected analyses were judged as acceptable or otherwise on the basis of spinel stoichiometry.

In some cases, plagioclase laths were small or thin plates with analysed MgO and FeO contents greater than 0.35 and 0.4% respectively. In these cases the 'best' analysis was selected on the basis of stoichiometry and low MgO and FeO.

Although olivine, orthopyroxene and plagioclase were generally large enough for consistent analyses (we aimed for five independent grain analyses), clinopyroxene characteristically formed abundant small euhedra. Where analyses of clinopyroxene showed a range of CaO contents we selected those with the highest CaO, recognizing the tendency in both experiments and natural rocks for subcalcic clinopyroxenes to appear with rapid growth or cooling. At 0.75 GPa in L21 and K89 we observed low-Ca clinopyroxene, which may be pigeonite, in addition to orthopyroxene and calcic clinopyroxene. The possible role of pigeonite was not explored further.

Glass compositions were analysed using 15 kV accelerating voltage and 1 nA beam current. There was no observable loss of Na between 'spot' and 'area scan' analyses of

glass in the most calcic glasses ( $\geq \text{An}_{80}$  plagioclase). In the Na-rich glasses, count-rates for Na radiation clearly decreased with time using spot mode of analysis. For intermediate and sodic glasses, 'area scan' analyses, usually of  $\geq 10 \mu\text{m} \times 12 \mu\text{m}$  areas, were obtained and spot analyses were not incorporated in the database. In Fig. 2 we illustrate (SEM images) typical experiments, and in Fig. 3 we plot single glass analyses. The homogeneity of glass composition in all oxides is summarized and most effectively illustrated in molecular normative projections (the basalt tetrahedron; Falloon *et al.*, 1988) where the small scatter of glass data (Fig. 3) provides the basis for confidence in both the experimental and analytical methods.

### Selection of experimental compositions

Previous experimental studies of melting of peridotite demonstrated modification of liquid compositions during quenching to glass by in-growth of thin quench rims on residual pyroxenes and olivine (Jaques & Green, 1980; Van Den Bleeken *et al.*, 2010). This problem is avoided in our experiments by obtaining experimental products with a high proportion, or large pools, of glass ( $>50 \mu\text{m}$ ). In addition, during electron beam micro-analysis of charges, it is necessary to confirm contact and continuity between liquid and all five phases. In seeking melt compositions on

Table 1: Starting compositions used in this study

	SiO <sub>2</sub>	TiO <sub>2</sub>	Al <sub>2</sub> O <sub>3</sub>	Cr <sub>2</sub> O <sub>3</sub>	NiO	FeO	MgO	CaO	Na <sub>2</sub> O	Mg#
<i>Residues series</i>										
Residue I (An <sub>80</sub> )	49.0	0.5	11.7	2.9	0.2	4.4	18.3	12.3	0.8	88.1
Residue IB (An <sub>80</sub> )	49.3	0.5	13.3	0.6	0.2	4.4	18.5	12.4	0.8	88.2
Residue II (An <sub>40</sub> )	52.4	0.5	9.3	3.0	0.2	4.4	18.4	9.6	2.3	88.2
Residue III (An <sub>0</sub> )	55.7	0.0	6.9	0.1	0.0	5.0	28.4	0.2	3.8	91.1
Enstatite (E4/BLT.1)	57.5	0.0	1.1	0.2	0.0	4.4	36.1	0.5	0.1	93.5
Olivine 89 (O5/2751)	40.6	0.0	0.1	0.0	0.0	10.4	48.9	0.1	0.0	89.4
<i>Liquid series</i>										
Liquid 1	48.6	1.0	18.5	0.4	0.2	6.3	10.5	14.6		74.8
Liquid 2	55.0	1.0	16.9	0.4	0.2	4.3	7.2	10.8	4.2	74.9
Liquid 3	59.4	1.0	18.6	0.4	0.2	2.3	4.3	3.6	10.2	76.9
Liquid 4	62.7	1.0	19.8	0.4	0.2	1.6	2.4		12.0	72.8
Liquid 5	59.4	1.3	17.5	0.5	0.5	3.4	4.1	3.9	9.4	68.2
Liquid 6	55.0	1.2	17.2	0.5	0.5	3.5	7.4	9.0	5.7	78.9
Liquid 7	52.0	1.2	16.9	0.5	0.5	5.2	9.7	13.5	0.5	76.9

Residues I or II are a mix of refractory mineral phases Ol(Mg#90) + Opx(Mg#90) + Cpx(Mg#90) + Plag(An<sub>80</sub> or An<sub>40</sub>) + Spinel(Mg#50 or Cr#80). The refractory mineral phases were combined in molecular proportions 5 Ol + 10 Opx + 10 Cpx + 10 Plag + 2 Sp, and 0.5 wt % TiO<sub>2</sub> was added to the mix. Residue IB is an Al-rich and Cr-poor Residue I. For Residue III the molecular proportions of refractory mineral phases consisted of 1/3Ol (Mg#89) + 1/3En + 1/3Ab. Liquid series: compositions of liquids from literature (L1 to L4) in equilibrium with four or five phases at 0.7 or 1 GPa, with addition of 1 wt % TiO<sub>2</sub> and 0.4 wt % Cr<sub>2</sub>O<sub>3</sub>, and of liquids from our early successful experiments (L5 to L7) in equilibrium with five phases at 0.75 GPa. Liquid 1 from Walter & Presnall (1994), 0.7 GPa, 1285°C, CMAS. Liquid 2 from Walter & Presnall (1994), 0.7 GPa, 1225°C, in equilibrium with Ol + Opx + Cpx + Plag(An<sub>58</sub>). Liquid 3 from T. J. Falloon *et al.* (unpublished data), 1 GPa, 1220°C, in equilibrium with Ol + Opx + Cpx + Plag(An<sub>22</sub>). Liquid 4 from Falloon *et al.* (1997), 1 GPa, 1220°C, in equilibrium with Ol + Opx + Albite. Liquid 5 from run K89 (1/3Residue II + 2/3L4 at 0.75 GPa, 1180°C). Liquid 6 from run K98 (1/3Residue I + 2/3L2 at 0.75 GPa, 1220°C). Liquid 7 from run L21 (2/3[(80%Residue I + 20%Ol89) + (80%L1 + 20%Ol89)] + 1/3L1, at 0.75 GPa, 1230°C).

a multiphase melt saturation surface, minerals may be in reaction with melt over short temperature intervals. It is thus possible to obtain charges in which melt compositions in some areas of a layered charge lie on the Opx + Cpx + Plag + Sp saturation surface (i.e. olivine absent) whereas olivine is present at the ends of the capsule and is armoured and separated from glass by Opx or Opx + Cpx. The compositions of such liquids are anomalous with respect to the five-phase + Liq dataset and are not included in our target compositions. However, the loss of one phase provides information on the trends of liquid composition diverging from particular compositions on the five-phase + Liq cotectic onto a related four-phase + Liq cotectic. Recognizing these complexities in the experiments, our selection of compositions and loading of capsules evolved to meet the objectives of ensuring large melt fractions and contact of melt with all five crystalline phases.

All experimental compositions were prepared as sintered oxide mixes rather than from crushed mineral mixes to avoid problems of mineral zoning or metastable persistence. Two sets of compositions, the L-series and R-series,

were prepared from high-purity oxides or carbonates (Na, Ca) thoroughly mixed and sintered at 1050°C (Table 1). The R-series compositions were calculated as a mix of relatively refractory minerals: Ol Mg<sub>90</sub>; Opx Mg<sub>90</sub>; Cpx Mg<sub>90</sub>; Plag An<sub>80</sub> or An<sub>40</sub>; Sp Mg<sub>50</sub>Cr<sub>50</sub> expressed in molecular proportions: [5Ol:10 Opx:10Cpx:10Plag:2Sp]. To maintain similarity to natural basalt and peridotite compositions by including a Ti-solid solution component, but to avoid saturating melts with a titanium-rich phase such as ilmenite or titanomagnetite, 0.5 wt % TiO<sub>2</sub> was also added to the mix. The L-series were compositions of liquids previously inferred to be saturated with four or five phases, including plagioclase, at 0.7 or 1 GPa; that is,

- L1—liquid from Walter & Presnall (1994) at 0.7 GPa, 1285°C (An<sub>100</sub>), CMAS;
- L2—liquid from Walter & Presnall (1994) at 0.7 GPa, 1225°C (An<sub>58</sub>), NCMAS;
- L3—liquid from T. J. Falloon *et al.* (unpublished data) at 1 GPa, 1220°C (An<sub>22</sub>);
- L4—liquid from Falloon *et al.* (1997) at 1 GPa, 1220°C [An<sub>0</sub> (NMA5)];

Table 2: *Experimental run data at 0.75 GPa*

Sample mount no.	Capsule type	Run no. for Au/Pd-3	<i>T</i> (°C)	Run time (h)	Initial sample composition (mixed or layered)	3-,4- or 5-phase assemblage with glass	AnPlag
M96	Au/Pd-3	D742	1240	24	mixed [1/2L7 + 1/2RIB] + Fo <sub>89</sub> at each end	Plag + Ol + Opx + Cpx + Sp	86.0
M97	Au/Pd-3	D742	1240	24	mixed [3/4L1 + 1/4RIB] + Fo <sub>89</sub> at each end	Plag + Ol + Opx + Cpx + Sp	94.0
M98	Au/Pd-3	D742	1240	24	mixed [1/4L1 + 3/4RIB] + Fo <sub>89</sub> at each end	Plag + Ol + Opx + Cpx + Sp	83.2
L21	Au/Pd-1		1230	72	layered 1/3L1 + 2/3[mixed (4/5RI + 1/5Fo <sub>89</sub> ) + (4/5L1 + 1/5Fo <sub>89</sub> )]	Plag + Opx + Cpx + Sp	93.0
M85	Au/Pd-3	D741	1230	24	mixed [1/4L1 + 3/4RIB] + Fo <sub>89</sub> at each end	Plag + Ol + Opx + Cpx + Sp	83.7
M86	Au/Pd-3	D741	1230	24	mixed [1/2L7 + 1/2RIB] + Fo <sub>89</sub> at each end	Plag + Ol + Opx + Cpx + Sp	84.2
M87	Au/Pd-3	D741	1230	24	mixed [3/4L1 + 1/4RIB] + Fo <sub>89</sub> at each end	Plag + Ol + Opx + Cpx + Sp	93.0
K98	Ol/Pt		1220	72	layered 2/3L2 + 1/3RI	Plag + Ol + Opx + Cpx + Sp	52.7
N55	Au/Pd-3	D796	1210	72	mixed [1/2L7 + 1/2RII] + Fo <sub>89</sub> at each end	Plag + Ol + Opx + Cpx + Sp	66.0
N56	Au/Pd-3	D796	1210	72	mixed [1/2L6 + 1/2RI] + Fo <sub>89</sub> at each end	Plag + Ol + Opx + Cpx + Sp	51.0
M13	Au/Pd-3	D684	1200	72	mixed [1/2L6 + 1/2RI]	Plag + Opx + Cpx + Sp	54.4
M14	Au/Pd-3	D684	1200	72	mixed [1/2L7 + 1/2RII]	Plag + Opx + Cpx + Sp	66.0
N62	Au/Pd-3	D798	1190	72	mixed [1/2L2 + 1/2RIII] + Fo <sub>89</sub> at each end	Plag + Ol + Opx + Cpx + Sp	30.3
N63	Au/Pd-3	D798	1190	72	mixed [1/2L4 + 1/2RII] + Fo <sub>89</sub> at each end	Plag + Ol + Opx + Cpx + Sp	28.4
K89	Ol/Pt		1180	72	layered 2/3L4 + 1/3RII	Plag + Ol + Opx + Cpx + Sp	19.9
N74	Au/Pd-3	D802	1180	72	mixed [1/2L3 + 1/2RII] + Fo <sub>89</sub> at each end	Plag + Ol + Opx + Cpx + Sp	18.4
N75	Au/Pd-3	D802	1180	72	mixed [1/2L5 + 1/2RII] + Fo <sub>89</sub> at each end	Plag + Ol + Opx + Cpx + Sp	19.8
N76	Au/Pd-3	D802	1180	72	mixed [1/2L4 + 1/2RII] + Fo <sub>89</sub> at each end	Plag + Ol + Opx + Cpx + Sp	21.5
K99	Au/Pd-1		1160	24	layered L4 + 10%Enstatite	Plag + Ol + Opx + Sp	0.4
L43	Ol/Pt		1160	72	layered L4 + 10%Enstatite	Plag + Ol + Opx + Sp	1.0
L59	Au/Pd-3	D-598	1160	24	layered 1/2L4 + 1/2R III	Ol + Opx + Sp	
L60	Au/Pd-3	D-598	1160	24	layered 1/2L5 + 1/2R III	Ol + Opx + Sp	
N64	Au/Pd-3	D798	1190	72	mixed [1/2L5 + 1/2RIII] + Fo <sub>89</sub> at each end	Ol + Opx + Sp	

Capsule type: Au/Pd-1, single capsule in one experiment; Au/Pd-3, three capsules in one experiment; Ol/Pt, one olivine capsule in one platinum capsule in one experiment. Initial sample composition: mixed indicates that liquid and residue starting mixes are thoroughly mixed before introduction into the capsule; layered indicates that liquid and residue starting mixes are added sequentially into the capsule. Abbreviations: Plag, plagioclase; Ol, olivine; Opx, orthopyroxene; Cpx, clinopyroxene; Sp, spinel. AnPlag, anorthite content of the analysed plagioclase after the experiment. *T* (°C), in the case of Au/Pd-3 capsule experiments, 20°C has been added to the nominal temperature.

L5—liquid from experiment K89 (this study), 0.75 GPa, 1180°C;

L6—liquid from experiment K98 (this study), 0.75 GPa, 1220°C;

L7—liquid from experiment L21 (this study), 0.75 GPa, 1230°C;

L7a—liquid L7 + 20% olivine Fo<sub>90</sub>.

In addition, all L-series compositions contained 10% TiO<sub>2</sub> and 0.4% Cr<sub>2</sub>O<sub>3</sub> to maintain compositions resembling natural phase assemblages.

Initially, layered experiments using selected R and L compositions were run in single-capsule runs with the expectation that the selected *P,T* would yield charges with a glass-rich end and a crystal-rich (five-phases + Liq) assemblage at the R-series end of the capsule. Very few

experiments (K89, K98; Table 2) were successful in yielding charges with all five residual phases + Liq with the latter penetrating among all residual phases. Most samples were glass-rich with spinel and one or more other phases at one end and crystal-rich at the opposite end with gradients in mineral assemblage; for example, lacking olivine close to the glass layer and lacking plagioclase and/or clinopyroxene where olivine occurred.

Some success was achieved by layered experiments with an L-series composition and a mixed (L + R) composition as the two layers (L21; Table 2), always in single-capsule runs (olivine or AuPd capsules; see Fig. 1). However, frequent absence of one or more phases (commonly plagioclase or olivine) from the glass-rich part of the charge (i.e. that part where liquid could be analysed without concern about quench growth of crystals or electron

beam overlap) meant uncertainty in demonstrating saturation by all phases. For the most sodic compositions (L43, K99; Table 2), enstatite only (in addition to L4) replaced R compositions in layered experiments

Finally, most success was achieved by a 'three-capsules in one large capsule' method (3–1 cps; Fig. 1) in which San Carlos olivine (Fo<sub>89–90</sub>) was added at both ends of each inner capsule and the reactant mixture of mixed L + R compositions located as the central layer of the charge (Table 2). By varying both proportions and compositions of L and R, small differences on bulk composition were achieved such that at a given *P*, *T*, we might expect to straddle the four-phase + Liq to five-phase + Liq transition.

Because of the method of varying bulk composition by mixing different proportions of the L- and R-series composition and by variable amounts of olivine, there is no attempt to use mass balance (six phases) to estimate phase proportions. Bulk compositions of each experimental run can be estimated from the weighing in of the mixed and olivine layers but weighing errors become significant. The variation of bulk compositions was an empirical means to obtain charges with small differences in bulk composition and with two or three of the 3-in-1 capsules containing the desired phase assemblage at the same *P* and *T*. The method differs from the common practice in peridotite melting studies in which the phase relations and melt compositions are explored for one or more selected lherzolite compositions.

The objective was to find glass-rich, well-crystallized five-phase + Liq assemblages in which all phases can be analysed, and continuity and constancy of liquid (glass) composition demonstrated, in contact with all phases. The method actually follows that of classical experimental petrology by varying compositions to map liquidus phase fields and cotectic relationships, seeking to define a six-phase field in 'natural' magma composition space.

## LINKS TO PREVIOUS STUDIES

In previous studies of lherzolite melting at mantle pressures there are few determinations of liquid compositions in equilibrium with five crystalline phases. Also, plagioclase is typically present only at or below the estimated solidus temperature. These studies provide a helpful starting point for estimating the liquid compositions of interest.

An alternative and complementary route to understanding peridotite melting behaviour is the investigation of chemical subsystems of increasing complexity. The present study builds on the work of Presnall *et al.* (1979) on the system CaO–MgO–Al<sub>2</sub>O<sub>3</sub>–SiO<sub>2</sub> (CMAS) defining the composition of liquid in the five-phase univariant assemblage Fo + En + Di + An + Liq at pressures where spinel is absent.

The additional components Na<sub>2</sub>O (NCMAS) and FeO (FCMAS) have been studied by Walter & Presnall (1994)

and Gudfinnsson & Presnall (2000). These components do not introduce an additional phase. They define vectors in compositional plots and projections illustrating the movement of a phase boundary attributable to the particular substitutions (Na–Ca, Fe–Mg). Therefore they add a further degree of variance; that is, the Fo + En + Di + An + Liq assemblage becomes divariant in *P*, *T* space, and univariant at a fixed pressure in each of these systems.

The addition of Cr<sub>2</sub>O<sub>3</sub> to CMAS adds an additional phase (Cr–Al Sp) provided that the amount of Cr<sub>2</sub>O<sub>3</sub> added is greater than can be accommodated in pyroxene solid solutions. The Fo + En + Di + An + Cr–AlSp + Liq assemblage is univariant in CMASCr. Liu & O'Neill (2004) investigated the assemblage Fo + En + Di + Sp + Liq in this system at a fixed pressure (1.1 GPa) over a range of Cr<sub>2</sub>O<sub>3</sub> contents (i.e. spinel compositions).

Because Fo + En + Di + An + Sp + Liq is invariant in the CMAS system, any bulk composition close to the invariant point will pass from above liquidus to sub-solidus over a very small temperature interval. By adding components that enter the mineral solid solutions, the five-phase + Liq assemblage is no longer invariant and the melting interval is extended. Nevertheless, the choice of bulk compositions close to the five-phase + Liq field means that large increases in degree of crystallization may be expected over small temperature intervals. Thus the use of three compositions differing principally in their Na/Ca ratio, at a particular *P* and *T*, is an attempt to improve the probability of having five phases + Liq present in at least one charge.

We present data from experiments where the proportion of glass to crystals is high and in the case of layered experiments, glass is well connected from glass-rich to crystal-rich ends.

## EXPERIMENTAL RESULTS

The experimental data on melt and coexisting minerals at 0.75 GPa are presented in Table 3 and plotted in Figs 4–16. In these figures, data points are identified as 'five phases + Liq' (filled symbols), 'Ol-absent' (open symbols), Cpx-absent (asterisk) and by symbol type indicating the experimental temperature. This presentation illustrates the compositional variance of melts and minerals, all of which have the 'five phases + Liq' assemblage at the same temperature.

Conceptually, the data illustrate how liquids may vary in composition along an isotherm in chemically heterogeneous lherzolite in which the same mineral phases are present but local bulk compositions differ. Melt and mineral compositions are constrained by complex continuous reactions among the coexisting phases.

Table 3: Experimental phase compositions at 0.75 GPa

T (°C)	Sample mount no.	Phase	Analysis type	SiO <sub>2</sub>	TiO <sub>2</sub>	Al <sub>2</sub> O <sub>3</sub>	Cr <sub>2</sub> O <sub>3</sub>	FeO	NiO	MgO	CaO	Na <sub>2</sub> O	Mg#	Ca#	Cr#			
1240	M96	Ol	A(5)	41.8(2)	0.03(5)		0.1(1)	7.9(2)	0.49(7)	49.4(1)	0.23(6)		91.8					
		Opx	A(9)	55.1(4)	0.21(8)	4.4(7)	1.3(3)	4.4(2)	0.3(2)	31.4(7)	2.7(3)	0.13(3)		92.7	16.7			
		Cpx	A(6)	52.4(3)	0.4(1)	5.6(4)	1.7(2)	3.1(3)	0.08(8)	19.2(9)	17.3(9)	0.29(6)		91.7	97.0	17.1		
		Plag	A(2)	48.3(4)	0.2(1)	30(2)	0.5(6)	0.8(2)		2(1)	16(1)	2(2)			86.0			
		Sp	C(6)		0.2(1)	35(2)	36(2)	8.4(3)			19.9(4)			80.9		40.9		
		Gl	A(13)	53.3(3)	1.0(7)	17.0(2)	0.18(5)	4.2(1)		10.0(3)	13.0(2)	1.10(5)		80.8				
		1240	M97	Ol	A(3)	41.5(3)	0.04(5)	0.28(6)	0.09(6)	7.7(6)	0.4(1)	49.7(3)	0.25(1)		92.0			
				Opx	A(5)	53.6(6)	0.26(4)	6.6(7)	1.2(2)	5.1(5)	0.2(1)	30.6(5)	2.5(1)	0.02(3)		91.5	10.6	
				Cpx	A(3)	52(1)	0.5(3)	6.4(7)	1.2(2)	3.2(3)	0.02(2)	20(1)	17(1)	0.03(3)		91.7	99.6	11.1
				Plag	A(6)	45.9(8)	0.03(6)	33.6(7)	0.05(8)	0.4(1)	0.08(8)	0.7(1)	18.5(2)	0.7(1)			93.8	
1240	M98	Sp	C(3)		0.4(2)	49(1)	20.2(7)	7.5(5)	0.2(4)	22.9(6)			84.5		21.7			
		Gl	A(5)	52.5(3)	1.4(1)	17.1(3)	0.2(1)	4.3(1)		10.3(4)	13.9(1)	0.38(2)		81.2				
		Ol	A(4)	41.7(2)	0.1(1)	0.18(7)	0.09(7)	7.6(4)	0.40(4)	49.7(3)	0.3(3)			92.1				
		Opx	A(11)	54.8(9)	0.18(6)	6(1)	0.7(2)	4.8(3)	0.2(2)	31.2(7)	2.6(3)			92.0	7.8			
		Cpx	A(9)	52.9(5)	0.36(8)	5.6(7)	0.9(1)	3.0(4)	0.08(8)	20.2(9)	16.8(9)	0.17(3)		92.4	98.2	9.5		
		Plag	A(10)	48.8(4)	0.07(6)	32.4(3)	0.09(5)	0.3(1)	0.1(1)	1(2)	16.3(2)	2(2)			83.2			
1230	L21	Sp	C(4)		0.2(2)	52(5)	20(2)	7(1)	0.06(8)	21(2)			84.9		20.2			
		Gl	A(10)	52.6(7)	1(1)	17.6(4)	0.1(1)	4.1(2)		10.0(5)	13.2(4)	1.2		81.4	92.7			
		1230	M85	Ol	A(6)	41.7(3)	0.03(3)	0.18(9)	0.07(2)	7(1)	0.3(1)	50.9(6)	0.25(7)		93.2			
				Opx	A(6)	55.4(7)	0.21(8)	4(1)	0.8(2)	4.0(4)	0.2(1)	32.5(4)	2.5(2)	0.02(4)		93.6	11.2	
				Cpx	A(6)	53.1(4)	0.25(4)	4.8(5)	1.0(2)	2.6(4)	0.02(4)	19.9(4)	18.1(5)	0.20(4)		93.3	98.0	11.7
				Plag	A(6)	48.1(4)	0.09(6)	32.2(4)	0.06(7)	0.3(2)	0.02(3)	0.8(2)	16.6(3)	2.0(2)			83.7	
		1230	M86	Sp	C(3)		0.3(3)	50(4)	19(3)	6.0(3)	0.2(4)	24.1(6)			87.8		20.4	
				Gl	A(9)	52.8(5)	1.2(1)	17.7(4)	0.10(7)	3.8(2)		9.6(3)	13.5(2)	1.3(1)		81.7	92.0	
				Ol	A(5)	41.6(3)	0.01(2)	0.25(2)	0.02(3)	8.6(4)	0.38(4)	49(2)	0.31(3)			91.0		
				Opx	A(10)	55.4(4)	0.22(8)	4.4(5)	1.0(1)	4.4(3)	0.3(1)	31.5(4)	2.7(2)	0.03(4)		92.7	13.5	
Cpx	A(12)			52.6(5)	0.4(1)	5.5(5)	1.5(2)	3.3(2)	0.2(1)	19.9(8)	16.6(9)	0.15(6)		91.6	98.4	15.3		
Plag	A(12)			48.7(5)	0.05(7)	31.6(5)	0.06(5)	0.5(1)	0.03(5)	1.0(4)	16.5(3)	2.0(2)			84.2			
1230	M87	Sp	C(5)		0.2(1)	35(2)	37(3)	9.3(5)	0.09(0)	18(2)			77.8		41.2			
		Gl	A(12)	53.1(2)	1.05(9)	16.9(2)	0.16(7)	4.9(1)		9.8(3)	13.0(2)	1.1(8)		78.1	93.2			
		Ol	A(3)	42.0(3)	0.02(2)	0.5(3)	0.1(1)	8.6(3)	0.3(2)	48.2(6)	0.3(2)			90.9				
		Opx	A(5)	54.9(9)	0.2(1)	4(1)	1.0(3)	5.7(1)	0.12(9)	31.2(6)	2.5(1)	0.01(3)		90.7	13.4			
		Cpx	A(6)	51.4(3)	0.4(1)	6.5(9)	1.6(3)	3.9(3)	0.05(5)	19.0(6)	17(1)	0.05(5)		89.6	99.5	14.0		
		Plag	A(4)	45.9(5)		33.8(3)	0.1(1)	0.4(6)	0.01(1)	1(2)	18.3(3)	0.71(5)			93.4			
		Sp	CS(1)		0.75	29.84	36.60	13.4		19.4				72.2		45.1		
		Gl	A(11)	51.7(4)	1.3(7)	16.8(1)	0.19(8)	6.0(2)		9.9(2)	13.7(2)	0.37(5)		74.9	97.6			
		1220	K98	Ol	A(3)	41.1(3)	0.03(0)	0.07(10)	0.19(2)	7.2(5)	0.17(4)	51.0(8)	0.28(4)				92.7	
				Opx	A(3)	55.2(5)	0.3(1)	3(1)	1.0(3)	5.5(2)	0.07(5)	32.3(8)	2.4(3)	0.16(2)		92.3	19.2	
Cpx	A(6)			52.8(5)	0.52(4)	4.3(4)	1.7(1)	3.4(3)	0.06(6)	20.5(8)	16.1(6)	0.7(1)		91.5	92.7	21.0		
Plag	A(4)			54.9(6)	0.05(3)	27.8(2)	0.09(6)	0.17(6)	0.2(1)	11.3(6)	5.6(2)			52.7				
Sp	A(3)			3.0(2)	0.8(1)	31.0(5)	36.9(3)	8.5(1)	0.01(0)	18.8(1)	0.93(5)	0.14(6)		79.7	44.4			
1210	N55	Gl	A(2)	55.5(1)	1.5(2)	17.2(1)	0.13(2)	3.5(1)		7.4(0)	9.0(1)	5.71(8)		78.9	95.2			
		Ol	A(4)	41.5(2)	0.04(3)	0.01(3)	0.07(8)	8.9(2)	0.44(5)	48.8(3)	0.23(2)			90.7				
		Opx	A(9)	54.8(2)	0.2(1)	4.3(3)	1.7(2)	5.5(3)	0.3(2)	30.4(5)	2.6(3)	0.03(7)		90.7	20.6			
		Cpx	A(9)	52.4(4)	0.5(1)	5.3(5)	2.2(1)	3.5(2)	0.07(8)	18.7(9)	16.8(6)	0.6(1)		90.6	94.4	21.8		
		Plag	A(3)	52.4(4)	0.04(4)	29.7(2)	0.14(6)	0.4(1)	0.08(7)	0.27(3)	13.2(2)	3.74(1)			66.0			
		Sp	C(9)		0.43(6)	27(1)	44(1)	11.5(3)	0.01(2)	17.2(3)				72.7		52.0		
		Gl	A(5)	55.0(3)	1(1)	16.6(1)	0.21(9)	4.9(3)		8.1(1)	11.4(2)	2.5(5)		74.6	83.3			

(continued)

Table 3: Continued

T (°C)	Sample mount no.	Phase	Analysis type	SiO <sub>2</sub>	TiO <sub>2</sub>	Al <sub>2</sub> O <sub>3</sub>	Cr <sub>2</sub> O <sub>3</sub>	FeO	NiO	MgO	CaO	Na <sub>2</sub> O	Mg#	Ca#	Cr#
1210	N56	OI	A(2)	42.4(3)		0.02(2)	0.08(1)	5.1(2)	0.2(2)	52.0(3)	0.26(3)		94.8		
		Opx	A(9)	55(1)	0.3(1)	5(1)	1.3(3)	4.0(5)	0.3(2)	32.1(9)	2.2(1)	0.18(7)	93.5		16.2
		Cpx	A(8)	52.9(3)	0.63(6)	5.4(7)	2.1(3)	2.2(3)	0.04(7)	19.2(6)	16.7(9)	0.8(2)	94.0	91.7	20.3
		Plag	A(7)	55.4(5)	0.12(7)	28.1(4)	0.09(5)	0.2(5)	0.02(2)	0.2(6)	10.3(3)	5.5(1)		51.0	
		Sp	A(6)	0.4(3)	0.64(9)	37(3)	35(4)	5.2(3)	0.1(2)	21.6(4)	0.2(1)	0.10(8)	88.1		39.2
		Gl	A(13)	56.2(3)	2(2)	17.8(2)	0.2(2)	2.0(2)		7.6(3)	8.6(1)	5.6(1)	87.1	88.3	
1200	M13	Opx	A(6)	54.7(5)	0.3(1)	4.5(6)	1.2(1)	5.2(4)	n.d.	31.6(4)	2.41(3)	0.14(7)	91.5		15.6
		Cpx	A(6)	52.1(7)	0.47(9)	5.1(8)	1.7(2)	3.9(2)	n.d.	19.2(6)	16.8(6)	0.7(1)	90.2	93.1	18.4
		Plag	A(6)	55(1)	0.1(1)	28.0(7)	0.17(5)	0.38(7)	0.4(1)	11.1(8)	5.1(5)		54.4		
		Sp	C(2)	0.6(1)	38(3)	29(2)	13(1)	n.d.	19.0(2)				72.0		34.3
1200	M14	Gl	A(4)	55.2(2)	1.4(8)	16.8(2)	0.11(3)	5.3(2)		7.2(2)	9.0(1)	5.0(1)	70.7	96.7	
		Opx	A(7)	54.7(8)	0.17(9)	4.1(6)	1.4(3)	6(1)	n.d.	31(1)	2.5(3)	0.03(4)	89.7		18.9
		Cpx	A(6)	51.7(5)	0.4(2)	4.9(8)	2.0(1)	4.8(4)	n.d.	18.0(4)	17.8(5)	0.44(5)	87.0	95.7	21.2
		Plag	A(5)	52.2(1)	0.06(4)	29.6(1)	0.03(2)	0.5(1)		0.34(4)	13.5(1)	3.7(1)		66.5	
		Sp	A(3)	0.6(2)	0.54(5)	26.1(7)	40.3(9)	17.0(5)	n.d.	15.0(2)	0.38(5)	0.14(4)	61.1		50.9
Gl	A(6)	53.9(2)	1.4(8)	16.0(2)	0.17(6)	7.4(2)		7.6(2)	11.0(2)	2.6(1)	64.8	82.6			
<hr/>															
T (°C)	Sample mount no.	Phase	Analysis type	SiO <sub>2</sub>	TiO <sub>2</sub>	Al <sub>2</sub> O <sub>3</sub>	Cr <sub>2</sub> O <sub>3</sub>	FeO	NiO	MgO	CaO	Na <sub>2</sub> O	Mg#	Ca#	Cr#
1190	N62	OI	A(7)	42.1(3)	0.05(4)		0.09(8)	7.2(4)	0.4(2)	49.9(3)	0.22(3)		92.5		
		Opx	A(4)	57.1(5)	0.3(2)	1.6(3)	0.52(8)	6.3(4)	0.4(2)	31.4(6)	2.3(2)	0.21(6)	89.9		17.9
		Cpx	A(4)	55.1(4)	0.4(2)	2.8(2)	0.9(1)	3.8(3)	0.1(2)	20.1(6)	15.7(3)	1.04(1)	90.4	89.3	17.5
		Plag	A(7)	60.7(9)	0.1(1)	24.5(6)	0.07(7)	0.29(6)	0.07(7)	0.3(2)	6.1(4)	7.8(1)		30.3	
		Sp	n.d.												
1190	N63	Gl	A(4)	59.0(2)	1.47(3)	18.0(3)	0.01(1)	2.8(2)		5.0(1)	4.9(1)	8.9(2)	76.2	38.0	
		OI	A(4)	41.9(1)	0.04(7)		0.21(8)	4.9(5)	0.22(8)	52.6(5)	0.19(4)		95.0		
		Opx	A(8)	56.3(3)	0.23(7)	2.2(3)	1.4(2)	5.0(2)	0.4(20)	31.8(4)	2.3(2)	0.5(1)	92.0		29.4
		Cpx	A(10)	54.3(5)	0.45(8)	2.8(5)	2.42(4)	2.1(4)	0.1(1)	20.0(6)	16.5(9)	1.4(2)	94.6	86.8	36.7
		Plag	A(8)	62(1)	0.08(6)	23.7(7)	0.08(4)	0.1(1)		0.3(1)	5.9(8)	8.2(5)		28.4	
1180	K89	Sp	C(8)	0.75(9)	18(2)	55(3)	7(1)	n.d.	19.1(3)			83.1		66.7	
		Gl	A(7)	60.8(2)	1.1(2)	18.1(3)	0.16(4)	1.40(2)	4.7(4)	3.8(2)	9.9(1)	85.5	30.0		
		OI	A(3)	40.5(7)	0.01(2)	0.1(2)	0.2(2)	10.0(1)	48.8(8)	0.4(4)		89.7			
		Opx	A(6)	55.8(7)	0.31(4)	2.3(3)	1.2(1)	5.7(4)	0.21(4)	32.3(9)	1.9(7)	0.29(9)	91.4		26.8
		Cpx	A(3)	53.8(1)	0.5(1)	3.4(3)	2.05(2)	3.9(3)	0.11(2)	19(1)	15.9(2)	1.2(2)	89.7	88.4	28.7
1180	K89	Plag	A(4)	64(2)	0.17(5)	22.1(5)	0.04(6)	0.17(9)	0.2(2)	4(1)	9.3(4)		19.9		
		Sp	C(4)	1.3(1)	17.4(9)	51(2)	14.8(3)	n.d.	15.3(9)				64.9		66.3
		Gl	A(4)	59.7(1)	1.4(1)	17.7(1)	0.14(9)	3.4(0)		4.2(1)	3.9(1)	9.5(2)	68.9	31.4	
		<hr/>													
T (°C)	Sample mount no.	Phase	Analysis type	SiO <sub>2</sub>	TiO <sub>2</sub>	Al <sub>2</sub> O <sub>3</sub>	Cr <sub>2</sub> O <sub>3</sub>	FeO	NiO	MgO	CaO	Na <sub>2</sub> O	Mg#	Ca#	Cr#
1180	N74	OI	A(5)	42.0(6)	0.06(4)	0.1(2)	0.2(1)	7(1)	0.4(2)	50.2(4)	0.19(8)		92.8		
		Opx	A(5)	56.7(3)	0.36(9)	1.8(3)	1.3(1)	5.0(2)	0.2(2)	32.0(4)	2.2(4)	0.42(4)	91.9		32.8
		Cpx	A(3)	54.4(3)	0.7(2)	3.0(4)	2.66(1)	2.8(2)	0.2(1)	18.9(6)	15.7(0)	1.64(1)	92.4	84.1	37.5
		Plag	A(5)	63.5(9)	0.2(1)	22.4(5)	0.2(2)	0.3(1)	0.11(7)	0.4(4)	3.8(6)	9.2(6)		18.4	
		Sp	C(4)	1.31(1)	15.8(6)	55.0(6)	11.5(8)	n.d.	16.4(5)				71.7		70.1
1180	N75	Gl	A(7)	60.9(3)	1.41(2)	18.2(2)	0.1(1)	2.13(2)	3.9(1)	3.0(1)	10.2(1)	76.6	24.8		
		OI	A(5)	42.0(4)	0.04(4)	0.03(5)	0.20(8)	6.9(6)	0.46(9)	50.0(5)	0.3(2)		92.8		
		Opx	A(5)	56.3(4)	0.37(6)	2.0(2)	1.3(1)	5.9(2)	0.4(2)	31.3(3)	2.0(1)	0.46(8)	90.4		30.0
		Cpx	A(5)	54.7(7)	1.3(1)	2.9(3)	1.93(5)	2.7(6)	0.3(2)	18(1)	16.2(9)	1.78(4)	92.4	83.4	30.7
		Plag	A(2)	63.1(6)	0.18(5)	22.9(2)	0.11(6)	0.19(6)	0.03(4)	0.17(9)	4.1(2)	9.2(2)		19.8	
1180	N76	Sp	C(4)	1.59(2)	16.2(5)	54(1)	11.8(5)	n.d.	16.6(2)			71.5		69.0	
		Gl	A(5)	60.6(3)	1.49(2)	18.3(4)	0.2(2)	2.0(1)		4.1(3)	3.4(1)	10.0(2)	78.3	27.1	
		OI	A(5)	42.0(8)	0.03(3)	0.01(3)	0.1(1)	8.9(2)	0.80(8)	48(1)	0.2(1)		90.6		
		Opx	A(8)	56.2(3)	0.6(2)	2.13(4)	1.33(1)	5.5(5)	0.3(1)	31.4(4)	2.1(3)	0.41(6)	91.0		29.5
		Cpx	A(3)	55(1)	0.9(6)	2.8(9)	2.25(5)	3.1(7)	0.2(1)	18.3(6)	16(1)	1.53(2)	91.3	85.6	35.2
1180	N76	Plag	A(7)	62.8(5)	0.23(9)	23.0(3)	0.1(1)	0.3(2)	0.04(5)	0.2(1)	4.4(4)	8.9(3)		21.5	
		Sp	C(7)	2.05(3)	16(2)	51(2)	15(1)	n.d.	16(1)			65.3		67.6	
		Gl	A(4)	58.8(3)	2.15(2)	18.0(5)	0.11(8)	3.2(3)		4.4(4)	4.1(1)	9.3(1)	71.0	32.6	
		<hr/>													

(continued)

Table 3: Continued

<i>T</i> (°C)	Sample mount no.	Phase	Analysis type	SiO <sub>2</sub>	TiO <sub>2</sub>	Al <sub>2</sub> O <sub>3</sub>	Cr <sub>2</sub> O <sub>3</sub>	FeO	NiO	MgO	CaO	Na <sub>2</sub> O	Mg#	Ca#	Cr#	
1160	K99	OI	A(4)	41.4(5)	0.07(6)	0.3(2)	0.05(5)	9(1)	1.3(4)	48(1)	0.04(5)		90.1			
		Opx	A(4)	58.2(2)	0.02(3)	0.77(1)	0.38(7)	4.3(1)	0.2(1)	35.4(1)	0.53(2)	0.18(5)	93.7		25.1	
		Plag	A(3)	67(2)	0.5(2)	20.4(3)	0.2(2)	0.4(2)		0.3(2)	0.07(7)	11(1)		0.4		
		Sp	C(2)		1.2(4)	6.3(3)	63(3)	17.9(0)	n.d.	12(1)				54.1		87.0
		Gl	A(3)		63.7(1)	1.3(1)	20.2(1)	0.1(1)	1.1(2)		2.1(1)	0.06(3)	11.4(1)	77.3	0.5	
1160	L43	OI	A(4)	41.4(2)		0.21(8)	0.06(6)	8(1)	0.3(3)	50(1)	0.07(4)			91.7		
		Opx	A(7)	57.7(9)	0.2(2)	2(1)	0.5(2)	4.5(6)	0.1(1)	35(1)	0.3(2)	0.3(3)	93.2		16.9	
		Plag	A(5)	67.7(4)	0.3(1)	19.6(1)	0.03(5)	0.17(6)	0.02(4)	0.2(1)	0.2(1)	11.7(1)		1.0		
		Sp	n.d.													
1160	L59	Gl	A(5)	63.2(1)	1.2(1)	20.3(1)	0.1(1)	1.3(2)		2.3(1)	0.03(3)	11.4(1)	76.1	0.3		
		OI	A(2)	41.2(1)			0.14(9)	8.1(2)	0.4(1)	50.0(2)	0.03(4)			91.7		
		Opx	S	58.1	0.05	0.53	0.26	4.6	0.22	35.9	0.19	0.1	93.3			
1160	L60	Sp	n.d.													
		Gl	A(4)	64.2(5)	0.8(3)	18.5(5)	0.01(2)	2.4(2)		3.2(3)	0.14(3)	10.8(4)	70.3			
		OI	A(2)	40.59(2)			0.04(6)	10.04(9)	0.49(2)	48.6(3)	0.11(1)			89.6		
		Opx	A(2)	57.9(1)	0.01(1)	0.88(1)	0.28(2)	4.5(2)		35.7(3)	0.50(1)	0.20(1)	93.4			
1160	L60	Sp	n.d.													
1160	L60	Gl	A(4)	60.4(4)	0.8(5)	17.9(6)	0.10(7)	3.9(2)		4.7(3)	3.1(2)	9.0(3)	68.1			

<i>T</i> (°C)	Sample mount no.	Phase	Analysis type	SiO <sub>2</sub>	TiO <sub>2</sub>	Al <sub>2</sub> O <sub>3</sub>	Cr <sub>2</sub> O <sub>3</sub>	FeO	NiO	MgO	CaO	Na <sub>2</sub> O	Mg#	Ca#	Cr#	
1190	N64	OI	A(5)	42.1(3)			0.17(8)	5.2(8)	0.2(1)	52.2(6)	0.15(2)			94.7		
		Opx	A(6)	58.4(2)	0.06(4)	0.68(7)	0.37(7)	4.5(2)		35.3(2)	0.53(5)	0.10(6)	93.3			
		Sp	n.d.													
		Gl	A(8)	61.3(1)	1.11(8)	19.0(1)	0.03(4)	1.7(3)	0.05(5)	4.0(2)	2.82(8)	10.0(2)	81.3			

*T* (°C), experimental temperature with a correction of +20°C for the 'three capsules in one large capsule' experiments. Analysis

type: A(5), average of five; C(2), average of two corrected analyses; S(1), selected single analysis; CS(1), selected corrected analysis selected because the spinel analysis required least removal of overlap of surrounding phase; n.d., not determined, because of small size of phase. OI, olivine; Opx, orthopyroxene; Cpx, clinopyroxene; Plag, plagioclase; Sp, spinel; Gl, glass (liquid).

### Glass compositions

Glass compositions correlate with temperature (Fig. 4) and show very good correlations among particular oxide pairs and ratios (Fig. 5). Oxide vs MgO correlations are strong for SiO<sub>2</sub>, CaO and Na<sub>2</sub>O but poor for FeO and Al<sub>2</sub>O<sub>3</sub>. The small apparent variation in TiO<sub>2</sub> (1–1.5%) within each group does not correlate with MgO variations. Cr<sub>2</sub>O<sub>3</sub> contents are at the limit of detection for our analytical conditions and apparently do not correlate with MgO.

### Olivine

Olivine compositions vary from Mg#<sub>90</sub> to Mg#<sub>95</sub>, with the compositions determined by the bulk composition and extent of melting within the charge. Within the Ca-rich melts, the olivines consistently have ~0.3% CaO, matching the values of olivine phenocrysts in basaltic magmas

of tholeiitic and alkali olivine basalt character. As we have not used optimal electron beam and analytical parameters to analyse for nickel, we have not attached any significance to the variability of NiO contents reported in Table 3.

### Orthopyroxene

In addition to Mg# variability, which parallels that in coexisting olivine, orthopyroxenes show variation in the Tschermak's silicate component [i.e. (2-Si or <sup>IV</sup>Al) in structural formulae] and in Cr content, assumed to enter orthopyroxene as CaCrAlSiO<sub>6</sub> or (MgFe)CrAlSiO<sub>6</sub>. Excellent positive correlations exist between the Cr# of orthopyroxene, coexisting clinopyroxene and spinel (Fig. 6a). Correlations between Cr<sub>2</sub>O<sub>3</sub> and Na<sub>2</sub>O contents of both orthopyroxene and clinopyroxene are also observed (Fig. 6e and f). In the CaO-absent compositions, our data

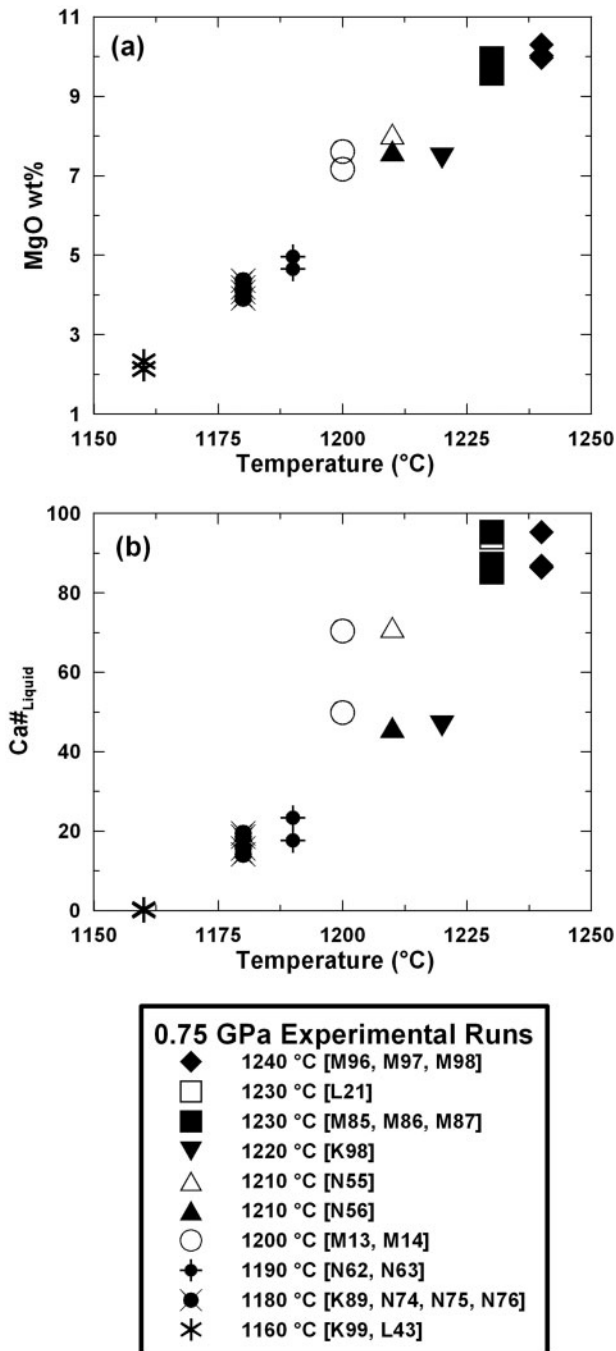


**Fig. 4.** Glass compositions (Table 3): correlations between nominal experimental run temperature and two significant chemical variables (a) MgO, (b) Ca# [CaO/(CaO+Na<sub>2</sub>O)] (mol). Symbols denote nominal run temperatures (see key) and are used in all subsequent figures. Filled symbols have five-phase + liq assemblages; open symbols lack olivine (opx + cpx + plag + sp + liq); asterisk (1160 °C) denotes absence of clinopyroxene (ol + opx + plag + sp + liq). It should be noted that the strong correlation of MgO with temperature implies similar correlations between temperature and other oxides as displayed against MgO in Fig. 5.

show a small NaCrSi<sub>2</sub>O<sub>6</sub> solid solution component in orthopyroxene in the absence of Cr-Tschermak's silicate solid solution. This component decreases with increasing Ca# in coexisting plagioclase. Some of these minor solid solution correlations are at or below accepted limits of detection by energy dispersive X-ray microanalysis (e.g. Na<sub>2</sub>O < 0.15 wt % in orthopyroxene). Nevertheless, the low concentration data are consistent with trends defined by higher concentrations in relevant phases.

### Clinopyroxene

Clinopyroxene demonstrates similar trends in Mg#, Tschermak's silicate and Cr# to orthopyroxene and spinel. The Ca# of clinopyroxene and the CaO content of orthopyroxene correlate with plagioclase An content and decrease from the calcic to sodic end of the five-phase + Liq cotectic (Fig. 6c). Marked positive correlations exist between the Cr# and Na contents of pyroxenes (Fig. 6e and f) and both are negatively correlated with Ca# of coexisting plagioclase (Fig. 6d). Also, <sup>IV</sup>Al<sub>cpx</sub> is positively correlated with the Ca# of plagioclase.

### Plagioclase

Plagioclase analyses in general demonstrate excellent stoichiometry provided that analysed MgO and FeO contents average <0.5 and <0.4 wt % respectively. A few examples departing from ideal stoichiometry are attributed to interference from enclosing glass. Ca and Na are used to calculate the An content, rather than using Si or Al values in the structural formulae.

### Spinel

Spinel proved to be the most difficult mineral to analyse, mainly because of its small grain size. Also, in some experiments, early crystallization of MgAl<sub>2</sub>O<sub>4</sub>-rich spinel and consequential reaction towards Cr-rich spinel led to mantling of MgAl<sub>2</sub>O<sub>4</sub>-rich spinel by plagioclase. In such cases preferred spinel compositions were those in glass or those with maximum (FeMg)Cr<sub>2</sub>O<sub>4</sub> content among the inclusions in plagioclase. For those spinels with initial analysed SiO<sub>2</sub> contents <1.5%, the calculation of spinel stoichiometry indicated low magnetite solid solution, consistent with low *f*O<sub>2</sub> conditions of ~FMQ to FMQ - 1 (where FMQ is the fayalite-magnetite-quartz buffer) for our experiments. Cr#<sub>sp</sub> and An<sub>plag</sub> correlate negatively (Fig. 6b). In detail the Cr#<sub>sp</sub> compositional field in the six-phase assemblage widens as An<sub>plag</sub> increases. Our data partially define the Cr#<sub>sp</sub> compositional variations between plagioclase-absent lherzolite and spinel-absent lherzolite fields on the Cr-rich and Na-rich sides respectively. Additional experiments that failed to crystallize plagioclase or spinel, and are thus 'failed' experiments for the purposes of this study, also help to limit the six-phase field. Clinopyroxene is absent in the most sodic compositions. The spinel coexisting with albite in the

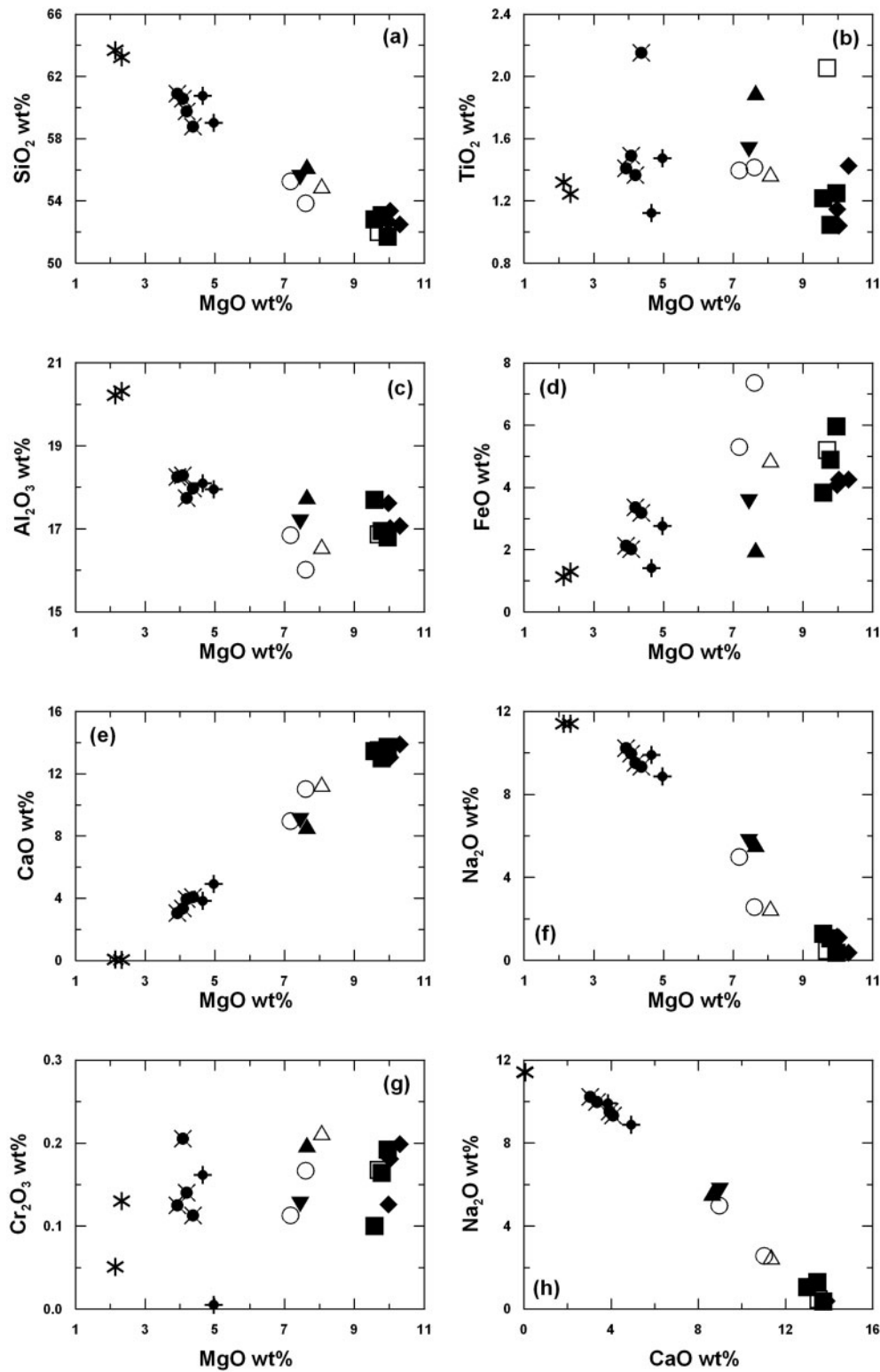


**Fig. 5.** Glass compositions (Table 3): correlations between oxides and MgO demonstrating the coherence of the dataset. It should be noted that the 'olivine-absent' experiments depart from the main trends in MgO vs SiO<sub>2</sub>, Al<sub>2</sub>O<sub>3</sub>, FeO, CaO and Na<sub>2</sub>O. Symbols as in Fig. 4.

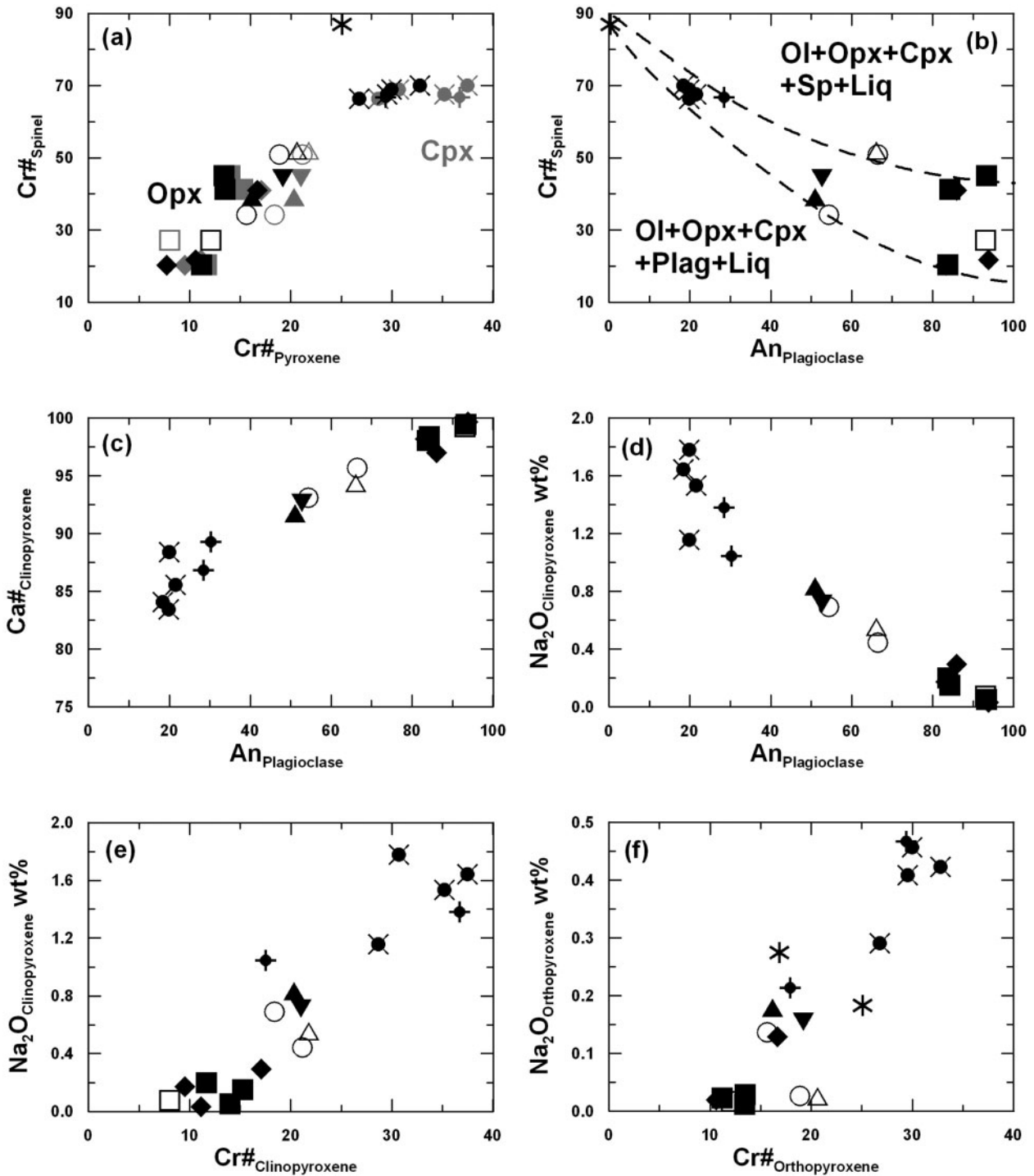


**Fig. 6.** Mineral vs mineral correlations demonstrating covariance interpretable in terms of solid solutions involving Ca–Na, Cr–Al, and AlAl–MgSi substitutions in plagioclase, pyroxenes and spinel. In (a) orthopyroxene compositions are black and clinopyroxene compositions are grey. In (b) the limiting of spinel compositions within the five-phase + liq assemblage between spinel-absent and plagioclase-absent fields is illustrated (see text). Symbols as in Fig. 4.

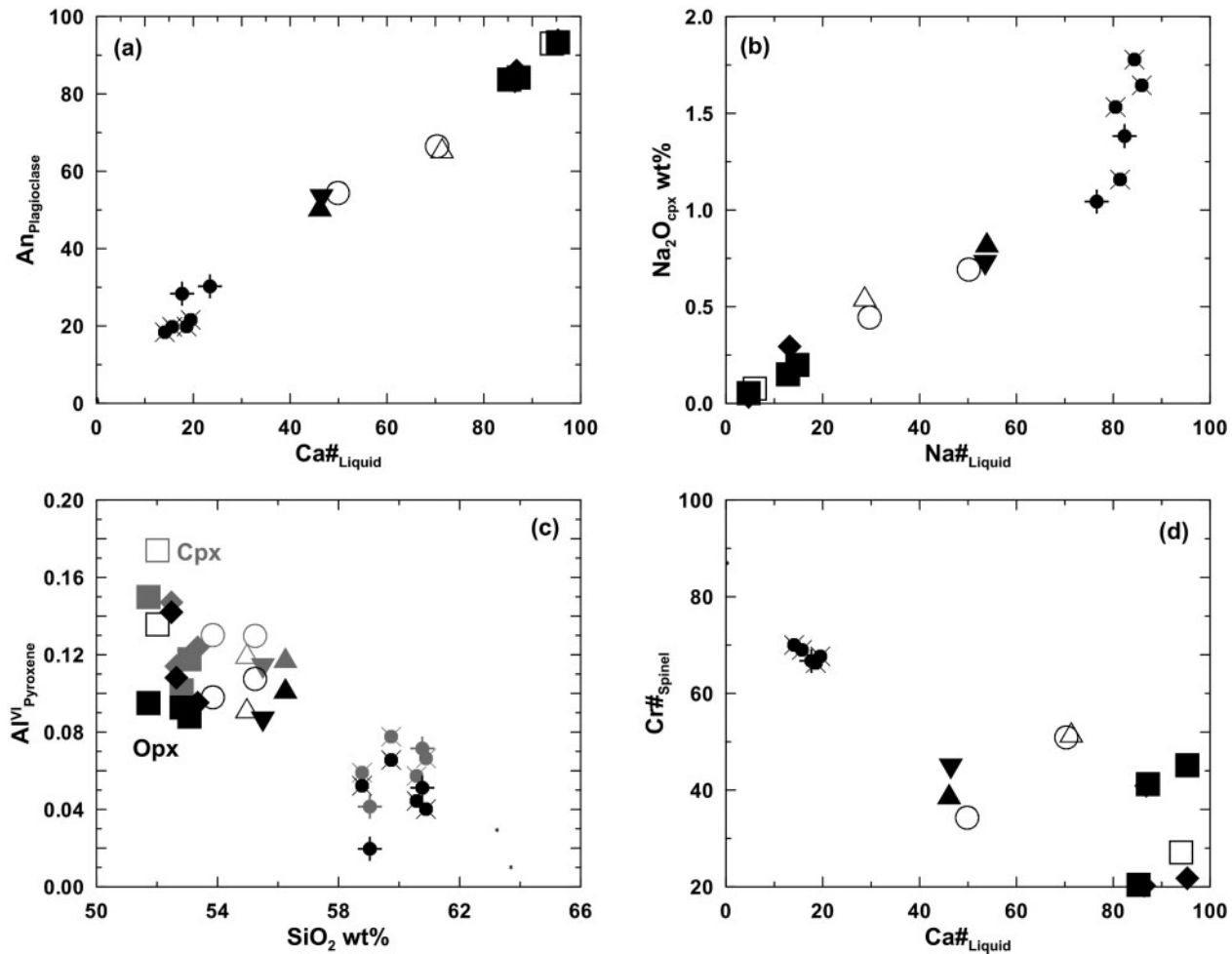
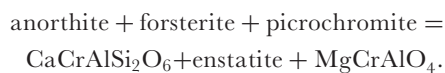
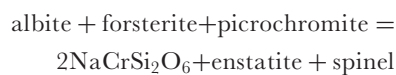


**Fig. 7.** Mineral vs liquid correlations demonstrating covariance between particular solid solution components in crystalline phases and concentration (SiO<sub>2</sub>) or major variable (Ca#, Na#) in the melt. It should be noted that (d) illustrates the same limitations to spinel composition in the five-phase + liq assemblages as noted in Fig. 6b. Symbols as in Fig. 4.

Ol + Opx + Plag + Sp + Liq assemblage is the most Cr-rich observed, at Cr<sub>87</sub>. This composition, together with the correlation between Na<sub>2</sub>O and Cr<sub>2</sub>O<sub>3</sub> in orthopyroxene and clinopyroxene noted previously, illustrates reactions such as



Such reactions among solid phases and within the liquid phase emphasize the variance within the natural system.

### Links between mineral solid solutions and glass compositions

Within the dataset for the composition of glasses that are multiply saturated (five phases) at 0.75 GPa

(Tables 2 and 3), the dominant correlation is between Ca/(Ca + Na) (Ca#) of glass and plagioclase. Temperature varies along the five-phase + Liq cotectic from 1240°C at the calcic end to 1160°C at the sodic end. Mineral compositions vary systematically along the trend with correlations between solid solutions in coexisting phases. At the sodic end of the five-phase + Liq compositional spectrum, the limiting composition of plagioclase is An<sub>18</sub>Ab<sub>82</sub>. For the most sodic compositions (Ab<sub>99-100</sub>) diopside is absent, and as the plagioclase changes from An<sub>18</sub>Ab<sub>82</sub> to An<sub>0</sub>Ab<sub>100</sub> the CaO content of orthopyroxene composition changes from ~2.2% at clinopyroxene saturation to 0% in the Ca-free system.

### Ca vs Na partitioning between glass and minerals

The positive correlation between An<sub>plag</sub>, Ca#<sub>liq</sub>, and T<sub>liq</sub> illustrates the dominant role of the plagioclase solid solution in determining the solidus temperature of the

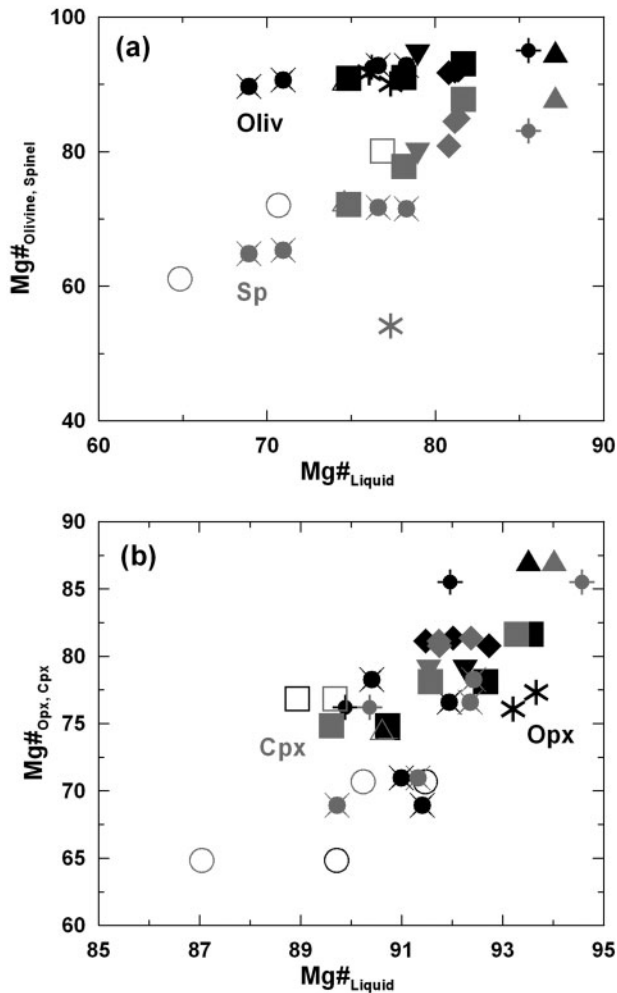


**Fig. 8.** Diagrams illustrating the Fe–Mg partitioning between liquid and olivine, and spinel (a), and between liquid and both orthopyroxene and clinopyroxene (b). Symbols as in Fig. 4.

spinel + plagioclase lherzolite assemblage (Figs 4b and 7a). Excellent positive correlations appear between the Ca# of glass and coexisting Ca- and Na-bearing phases including plag, cpx and opx (Figs 6 and 7).

#### *Mg–Fe partitioning between glass and minerals*

Good positive correlations appear between the Mg# of glass (liquid) and all coexisting ferromagnesian minerals (Fig. 8). Although for a single composition we expect the Mg# of glass and coexisting minerals to increase with increasing temperature, our approach of changing bulk compositions to locate the six-phase field means that at a given temperature we may have a range of Mg# in both glass and minerals, reflecting the extent of partial melting in different bulk compositions.

Thus our experimental strategy of maximizing the variation in Na/Ca of bulk compositions and maintaining

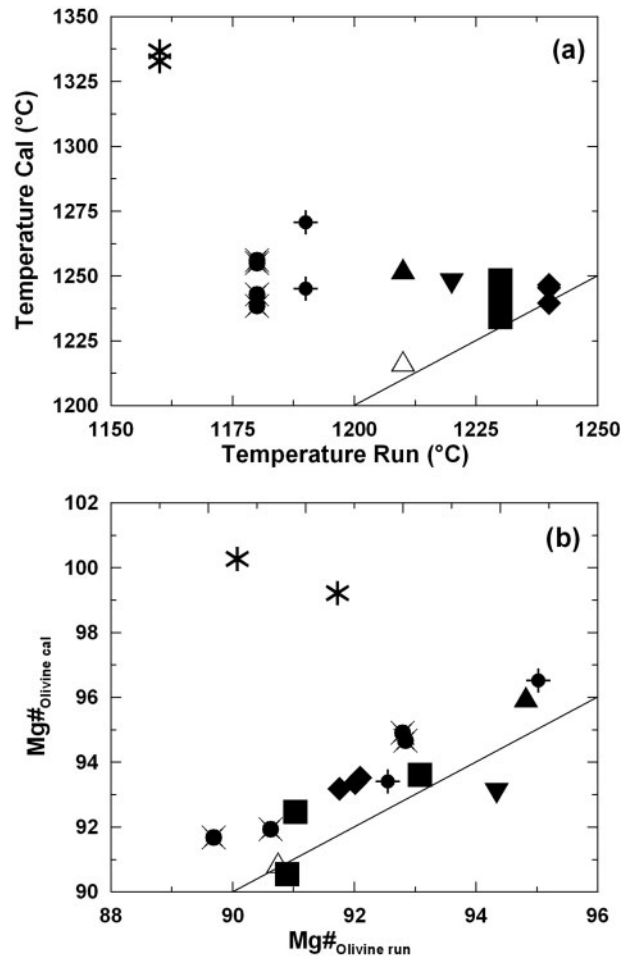


**Fig. 9.** Relationships between experimental temperatures and calculated temperatures using the olivine–liquid Fe–Mg relationship of Herzberg & O'Hara (2002), showing that only the calcic liquids agree in temperature values (a) whereas there is fairly good agreement between observed and predicted composition for all except the Ca-free compositions (b). Symbols as in Fig. 4.

Mg# near 90 means that we do not observe a good correlation between  $T$  and Mg# of glass or minerals. For the same reason, and also because of the marked difference in molecular weight between MgO and FeO, we observe only a poor correlation between MgO and FeO in oxide (wt %) plots of the glass compositions (Fig. 5d).

## COMPARISONS BETWEEN THE EXPERIMENTAL MINERAL–GLASS CORRELATIONS AND PREDICTIVE MODELS

### **Crystallization $T$ and Mg# of olivine**

Our data for the highest temperature ( $>1225^{\circ}\text{C}$ ) and most calcic compositions ( $\text{An}_{\text{plag}} \geq 80$ ;  $\text{CaO}_{\text{melt}} = 8\text{--}14\%$ ;

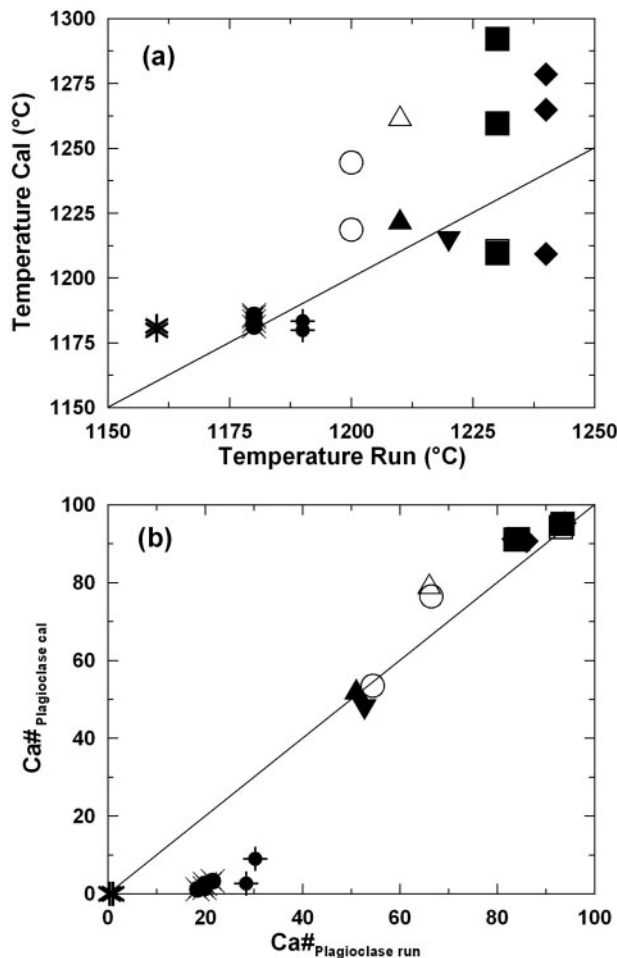


**Fig. 10.** Relationships between (a) experimental temperatures and calculated temperatures, and (b) experimental and calculated plagioclase compositions for plagioclase–glass pairs, using the model of Ariskin & Barmina (1990) (see text). Symbols as in Fig. 4.

$\text{MgO}_{\text{melt}} = 7\text{--}11\%$ ) are a good fit to the empirical models relating crystallization  $T$  and  $\text{Mg}\#$  of olivine (Ford *et al.* 1983; Herzberg & O'Hara, 2002) (Fig. 9). The model-predicted  $T$  is similar to or, at most,  $10^\circ\text{C}$  higher than the experimental  $T$ . However, the predicted  $T$  does not fit the experimental crystallization  $T$  of olivine in intermediate and sodic melts ( $\text{An}_{\text{plag}} \leq 55$ ;  $\text{CaO}_{\text{melt}} \leq 5\%$ ;  $\text{MgO}_{\text{melt}} \leq 5\%$ ). Indeed, these last data fall outside the range of the database used for calibration by Herzberg & O'Hara (2002). Also, the predicted olivine  $\text{Mg}\#$  is similar to or higher by 1–2 units than the experimental olivine  $\text{Mg}\#$  in both the calcic and sodic groups. Similar conclusions apply if the models of Ford *et al.* (1983) or others are used, suggesting that current models of olivine–liquid equilibrium do not adequately address intermediate to sodic liquids.

### Crystallization $T$ and $\text{An}_{\text{plag}}$

We have compared our experimental data for composition and temperature for plagioclase–glass pairs with the empirically derived model of Ariskin & Barmina (1990) (Fig. 10). Observed and predicted temperatures are in fairly good agreement for sodic glasses and plagioclase but not for calcic compositions. Conversely, predicted plagioclase compositions are in good agreement with experiments for calcic compositions ( $\text{An}_{\text{plag}} \geq 50$ ) but not for sodic compositions. These comparisons suggest that our new experimental data may be useful in modifying existing models of melt–plagioclase equilibrium.

## MELT COMPOSITIONS IN THE CRNFCMAS SYSTEM AND COMPARISONS WITH SIMPLER CMAS, NCMAS AND FCMAS SYSTEMS

### Melt compositions from this study in the CrNFCMAS system

We have demonstrated above the correlations between oxide concentrations and ratios in melts and mineral solid solutions showing that in the 'natural' chemically complex system, the compositions of the multiply saturated melts in plagioclase + spinel lherzolites have restricted compositions, varying continuously, and are particularly sensitive to the composition of plagioclase. This suggests that the most informative presentation of our data is based on normative mineralogy using the normative components olivine, diopside–hedenbergite, plagioclase and quartz (the CIPW norm).

As normative mineral solid solutions have defined stoichiometry and to avoid the distracting effects of different molecular weights for magnesium and iron end-members, or sodium and calcium end-members of solid solutions, we use a molecular rather than weight per cent expression of the CIPW norm. Our liquid compositions are expressed in molecular proportions of standard mineral end-members rather than as oxide percentages.

Finally, because our liquid compositions vary continuously from silica oversaturated and quartz-normative to silica undersaturated and nepheline-normative, we plot the data within the tetrahedron Olivine (Ol)–Diopside–Hedenbergite (Di)–Quartz (Qz)–(Jadeite (Jd) + Calcium Tschermak's silicate (CaTs) + Leucite (JCL), projecting from either the Di or Ol apex onto the opposite face.

The use of the normative projection also facilitates comparison between the cotectic in the CrNFCMAS system and cotectics and phase boundaries in the simpler systems such as CMAS, NCMAS and FCMAS.

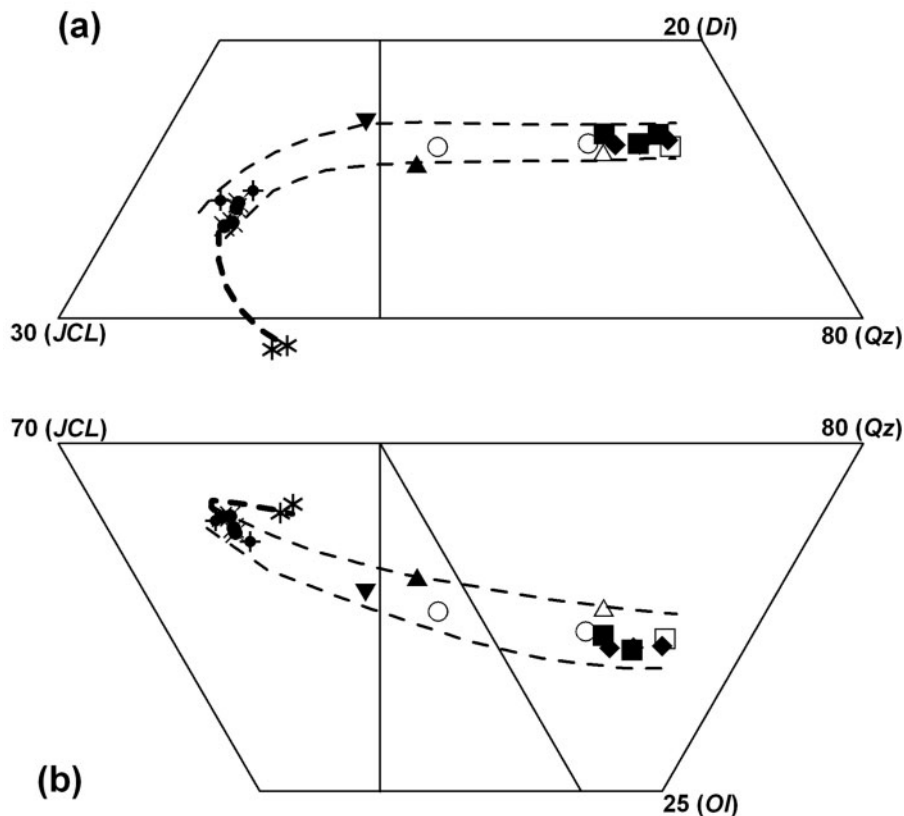


**Fig. 11.** Glass compositions from Table 3 and Figs 3–10, projected into the normative basalt tetrahedron, illustrating the relatively narrow compositional variation of the liquids on the plagioclase lherzolite five-phase + liq cotectic and their transition from quartz-normative to nepheline-normative compositions (i.e. crossing the Di, Ol, Plag plane). It should be noted that the five-phase + liq field terminates at the most silica-undersaturated glasses and the bold dashed line links to the Ca-free data points (\*) along an Ol + Opx + Plag + Sp + Liq cotectic with decreasing CaO in orthopyroxene and glass. The light dashed lines are drawn to limit the five-phase + liq field indicating positions with different Mg# [contour separation (i.e. from olivine of Mg<sub>94</sub> to Mg<sub>89</sub>) is in the same direction but appears greater than the FCMAS regression of Gudfinnsson & Presnall (2000)]. Symbols as in Fig. 4.

When projected into the basalt tetrahedron (Figs 3 and 11–15), the data illustrate liquid compositions on the ‘five-phase + Liq’ cotectic between 1240°C and 1180°C from An<sub>94</sub> to An<sub>18</sub>. At 1160°C and An<sub>1</sub>, Di did not crystallize and the liquid composition is on the ‘four-phase + Liq’ cotectic. The liquid compositions define a compositional band (see Fig. 11) rather than a line. This is due to the respective effects of Ca–Na, Mg–Fe and Cr–Al exchanges at *T* decreasing from 1240° to 1180°C.

### Comparisons with CMAS, NCMAS, FCMAS experiments at 0.75 GPa

The trend in the complex system (our results) is in agreement with that in the NCMAS system (Walter & Presnall, 1994) and our new data extend to more sodic liquids than previously explored. Also, in the complex system, liquids on the five-phase + Liq cotectic are displaced towards the Qz apex in the projection from Di relative to the four-phase + Liq cotectic (spinel absent)

defined by the CMAS and NCMAS data. With the addition of Cr<sub>2</sub>O<sub>3</sub> in excess of that which can be accommodated in pyroxene solid solution, we introduce an additional phase, Cr–Al spinel. This additional phase causes a significant shift from the ‘four-phase + Liq’ cotectic (spinel absent) in NCMAS to the five-phase + Liq cotectic in the complex system. The latter cotectic is expected to be applicable to natural rocks in which spinel with a variable Cr# is a characteristic accessory or minor phase.

The experimental data on mineral compositions demonstrate that the major solid solutions are: Na vs Ca in plagioclase, but also observable in pyroxenes; Fe vs Mg in olivine, pyroxenes and spinel, but deliberately restricted by our choice of compositions; and Al vs Cr in pyroxenes and spinel. In attempting to understand relationships between melt compositions and mineral compositions, the effects of these solid solutions are interactive and cumulative.

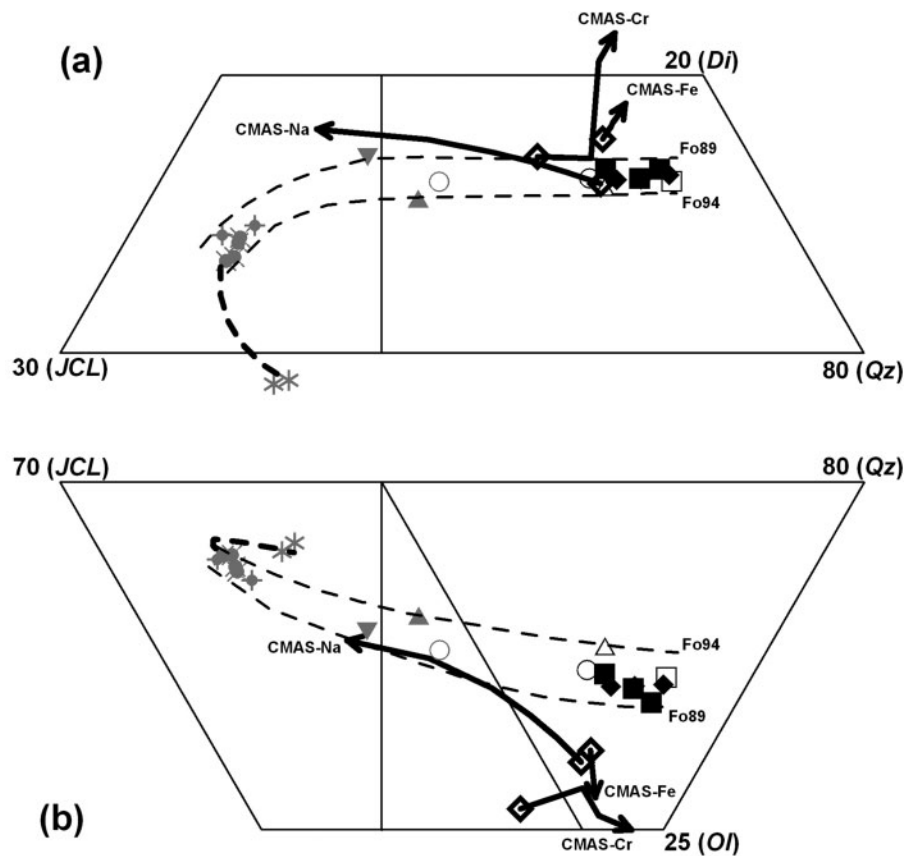


**Fig. 12.** As for Fig. 11 with the addition of the CMAS four-phase + liq invariant points at 0.75 GPa from the regressions of Gudfinnsson & Presnall (2000) in FCMAS (CMAS-Fe) and Walter & Presnall (1994) in NCMAS (CMAS-Na), and the CMAS four-phase + liq invariant point at 1.1 GPa (CMAS-Cr) from Liu & O'Neill (2004). In each case a vector is drawn from the CMAS invariant point along the four-phase + liq cotectic with increasing Fe, Na or Cr in olivine, plagioclase or spinel respectively. The vectors show the movement from  $Fo_{100}$  to  $Fo_{90}$  in the FCMAS system,  $An_{100}$  to  $An_{55}$  in the NCMAS system and  $Cr_0$  to  $Cr_{50}$  in the CrCMAS system. Comparing the simple systems with the complex system, which must integrate the complementary effects of each of the additional components, it is evident that the dominant effects on melt compositions relative to the CMAS system are the addition of another phase (aluminous and chromian spinel), resulting in significant shift of the four-phase + liq cotectic in CMAS to the five-phase + liq cotectic in the complex system, and the dominant role of the plagioclase solid solution in determining the normative compositions and degree of silica undersaturation of liquids in equilibrium with spinel-bearing plagioclase lherzolite. Symbols as in Fig. 4.

In this section we refer to experimental studies that have demonstrated the effects of each substitution on the CMAS six-phase invariant point and use this information to qualitatively interpret the observed shifts in melt composition in the complex composition.

Figure 12 illustrates the composition of liquid in equilibrium with forsterite, enstatite, diopside and anorthite (CMAS system) at 0.7–0.75 GPa from three related studies: CMAS (Presnall *et al.*, 1979), NCMAS (Walter & Presnall, 1994) and FCMAS (Gudfinnsson & Presnall, 2000). The small differences in the position of the invariant point for CMAS at 0.75 GPa reflect the different regressions derived for the univariant curve in the NCMAS and FCMAS systems. These curves are plotted for  $An_{100}$  to  $An_{55}$  in the NCMAS system and for  $Fo_{100}$  to  $Fo_{90}$  in the FCMAS system. There is a significantly higher normative

diopside content in the position of the invariant point calculated for  $An_{100}$ ,  $Fo_{100}$  derived from the FCMAS data than that derived from the NCMAS study (illustrated in the projection from olivine, Fig. 12a). However, the data overlap in the projection from diopside (Fig. 12b). Each of the projections illustrates the 'vector' of compositional change of liquid from the CMAS point with increasingly sodic plagioclase and increasingly iron-rich olivine. The movement of the  $OI + Opx + Cpx + Sp + Liq$  univariant boundary at 1.1 GPa in the CrCMAS system from Liu & O'Neill (2004) is also plotted, beginning at the CMAS point calculated for this pressure, and moving with increasing Cr#. The new experimental data are examined using the approximation that the compositional 'vector' derived in this study at 1.1 GPa is also applicable as a Cr# vector at 0.75 GPa.

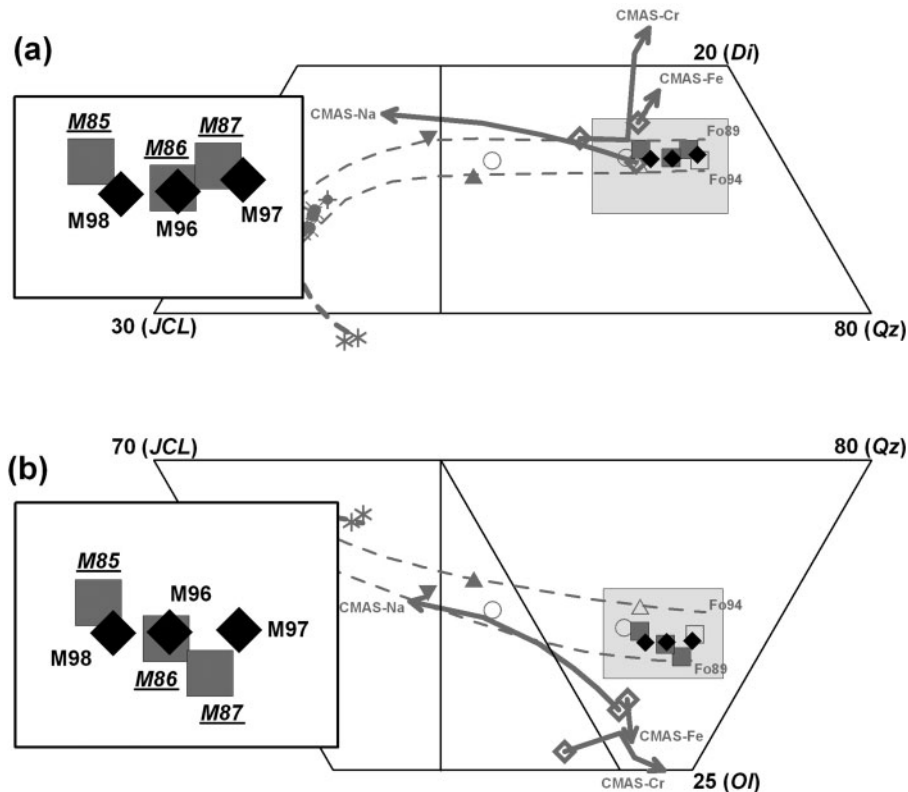


**Fig. 13.** As for Fig 12, illustrating the text discussion of the causes for the compositional differences between liquids saturated with anorthite-rich plagioclase from two sets of 3-in-1 capsules; that is, three experiments at 1240°C (M96–98) and three experiments at 1230°C (M85–87) in which the compositions of plagioclase, spinel, pyroxenes and olivine also vary within small ranges. As the temperature difference is within experimental uncertainty, the different liquid compositions should be consistent with the compositional shifts in the coexisting minerals (see text). Symbols as in Fig. 4.

In summary, in comparing the new data with FCMAS, NCMAS and CrCMAS data, the dominant effect of the plagioclase solid solution is confirmed. An additional very significant shift of liquids to more siliceous compositions (higher normative quartz) is attributed to the appearance of an additional phase (chrome–alumina spinel). Indeed, when comparing six-phase assemblages at 0.75 GPa with liquids on the Ol + Opx + Cpx + Plag + Liq cotectic (spinel-absent in Cr-absent compositions), the latter are less siliceous and plot closer to olivine or hypersthene in the normative tetrahedral plots. We expect that as Cr<sub>2</sub>O<sub>3</sub> concentration increases and enters pyroxene solid solutions, liquids move with the four-phase + Liq surface towards the spinel-bearing five-phase + Liq surface in compositional space.

#### Importance of Na/Ca, Fe/Mg and Cr/Al exchanges between liquid (glass) and coexisting minerals in a complex system

In the following discussion, the new data are examined for evidence of shifts in liquid composition attributable to the

Na/Ca, Fe/Mg and Cr/Al ‘vectors’ defined in the simple system studies.

Six experiments constrain the six-phase cotectic (solidus) at 0.75 GPa for lherzolite with An<sub>80</sub> to An<sub>95</sub> plagioclase, magnesian olivine and chrome–alumina spinel (Fig. 13). The six experiments (M85, M86, M87 and M96, M97, M98) are from two of the 3-in-1 capsules nominally run at 10°C difference in temperature. The relative plotting positions of these liquid compositions should be interpretable in terms of Na vs Ca, Mg vs Fe, and Al vs Cr exchanges between the liquid (glass) and coexisting minerals.

M98 and M85 have plagioclase of An<sub>83.2</sub> and An<sub>83.7</sub> respectively, olivine and pyroxenes with Mg# of ~92 and ~93.5 respectively, and Cr# of spinel of 20.2 and 20.4 respectively. The plotting positions of their glass compositions in the tetrahedral projections are overlapping. M96 and M86 glass compositions also overlap with each other in the tetrahedral plot. They have plagioclase of An<sub>86</sub> and An<sub>84.2</sub> respectively, olivine and pyroxenes of Mg<sub>91–92</sub>, but a different spinel (Cr# = 41) from the previous pair. The shift from the M98–M85 pair position to the M96–M86

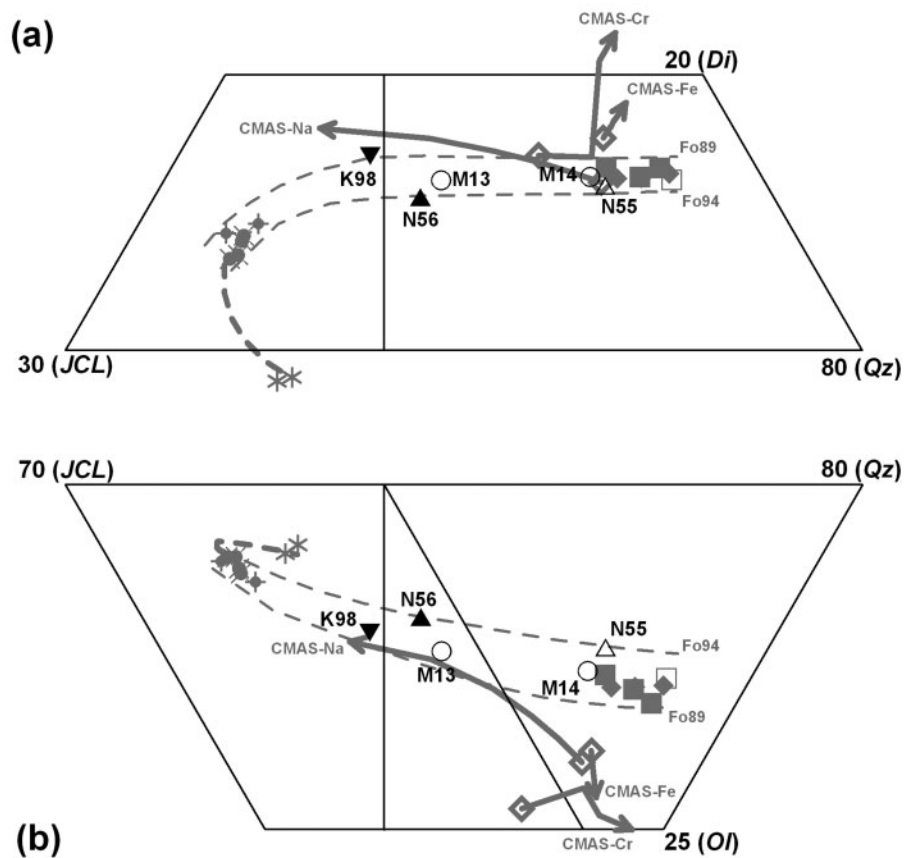


**Fig. 14.** As for Figs 12 and 13, illustrating the text discussion of the causes for the compositional differences between liquids saturated with intermediate plagioclase. The anomalous position of the liquids from N55 ( $An_{66}$ ) and M14 ( $An_{67}$ ) is apparent and these liquids are not in equilibrium with olivine but lie on  $Opx + Cpx + Plag + Sp + Liq$  cotectics (see text). Symbols as in Fig. 4.

pair position is attributable to the slightly more calcic plagioclase, more iron-rich olivine and pyroxenes, and more chrome-rich spinel in the M96–M86 pair; that is, a compositional shift resulting from three small composition vectors materializing the exchanges Na vs Ca, Mg vs Fe, Al vs Cr.

Also, M97 has olivine, pyroxenes and spinel with Mg# and Cr# matching M98. Thus the shift from M97 to M98 glass compositions must be attributed to their markedly different plagioclases (respectively  $An_{93.8}$  and  $An_{83.2}$ ). This means that the data ‘calibrate’ a shift of the pseudo-invariant point owing to 10 mol % An. M87 has Cr# in spinel and Cr# in pyroxenes that are similar to those in M96 and M86. However, M87 is more iron rich and has more calcic plagioclase ( $An_{93.4}$  compared with  $An_{86}$  and  $An_{84.2}$ ). The shift of M87 glass relative to the M96–M86 pair is thus consistent with a resultant from the plagioclase Ca# vector and the olivine and pyroxenes Mg# vector.

Turning to compositions with intermediate plagioclase composition (Fig. 14), N56 and K98 have plagioclase of

$An_{51}$  and  $An_{53}$  respectively. They have very similar Cr# in spinel and both pyroxenes. Olivine, pyroxenes and glass have lower Mg# in K98 than in N56. Three other experiments have intermediate plagioclase compositions. N55 and M14 have  $An_{66}$  plagioclase, very similar spinel ( $Cr\#_{52}$  and  $Cr\#_{51}$ ) and pyroxenes with similar Cr#. They differ from each other only in Mg# in pyroxenes and glass. However, the glass compositions are very different from those in K98 and N56, with much lower  $Na_2O$  contents. M14 does not contain olivine. Although N55 has olivine, it is only at the capsule ends and is separated from the glass-rich area by orthopyroxene. We suggest that despite the glass-rich character of part of the charge, the glass is in equilibrium with a ‘gabbroic’ (olivine-absent) residue. Therefore both N55 and M14 glasses are inferred to be on the  $Opx + Cpx + Plag + Sp + Liq$  cotectic. Plagioclase is more calcic and spinel more Cr-rich than phases on the five-phase +  $Liq$  cotectic at  $\sim 1210^\circ C$ . Also, pyroxenes and liquids are more Fe-rich than liquids at the same temperature but on the five-phase + liquid cotectic. Olivine is absent from M13 glass. Relative to N55 and

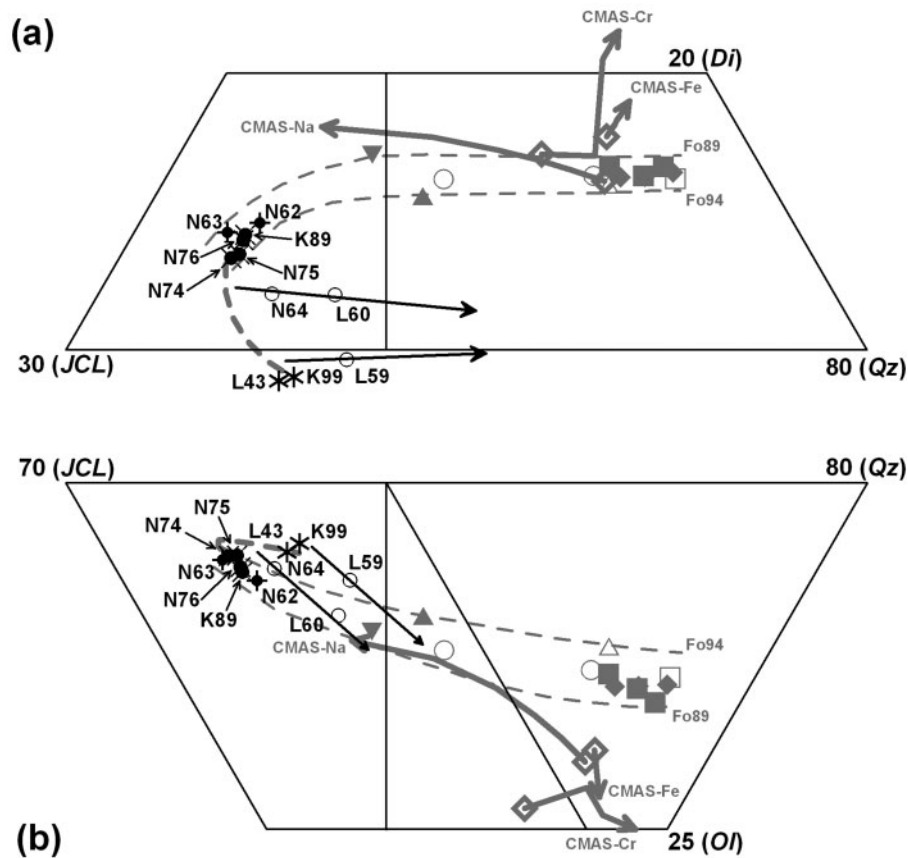


**Fig. 15.** As for Figs 12–14, illustrating the text discussion of the causes for the compositional differences between liquids saturated with sodic plagioclase, including liquids in the Ca-free system in which clinopyroxene is absent. The small open circles are liquids (see text) that are not saturated in plagioclase or clinopyroxene (i.e. spinel harzburgite residues) but in which different CaO contents and temperatures demonstrate movement of liquids off the five- or four-phase + liq cotectic towards refractory harzburgite residues. Symbols as in Fig. 4.

M14, M13 contains a more sodic plagioclase ( $An_{54}$ ), glass and pyroxenes with a higher Mg#, and spinel and pyroxenes with a lower Cr#. M13 glass and plagioclase are very similar to those of N56 and K98. The M13 glass plotting position is consistent with the differences in Mg# and Ca# from these experiments. It appears that although olivine is not present, the liquid in M13 has moved very little from the olivine-saturation surface.

At the sodic end, N74, N75 and N76 (3-in-1 capsule experiment) include very similar mineral assemblages with small shifts of glass compositions attributable to Mg# and Ca# vectors as defined in the more calcic compositions (Fig. 15). K89 and N75 have very similar plagioclase and spinel. The small K89 shift is attributed to the Fe vector. At a slightly higher temperature, N63 has more calcic plagioclase and more magnesian olivine and pyroxenes but the same spinel Cr# as N76. The shift in glass compositions is consistent with Mg# and particularly Ca# vectors. In N62, glass analyses are abnormally spread. Selection of the group with lowest normative

jadeite gives a glass composition consistent with the other compositions. Spinel was not analyzable. On the basis of the lower Cr# in both pyroxenes of N62 relative to N63, we infer that spinel in N62 has lower Cr# than N63.

K99 and L43 experiments were single-capsule experiments in AuPd capsules (24 h) and ‘olivine in AuPd’ capsules (3 days) respectively. As these experiments had only a minor CaO content (from the natural orthopyroxene used in the starting mix) diopside is absent. The liquid no longer lies on the diopside-saturation surface (Fig. 15). Glass and mineral compositions in the two runs are very similar. In the projection from olivine, they lie on the corundum-normative side of the join  $Qz(Hy)$  to  $(Jd + CaTs)$ . Spinel in K99 is very Cr-rich. Spinel in L43 was not analyzable. It is inferred that with decreasing CaO contents in orthopyroxene and the absence of clinopyroxene, liquids saturated with  $Ol + Opx + Plag + Sp$  would vary with plagioclase from  $\sim An_{18}$  to  $An_0$  as CaO content in orthopyroxene decreased from  $\sim 2.1\%$  (N74–N76) to 0% (Fig. 15).

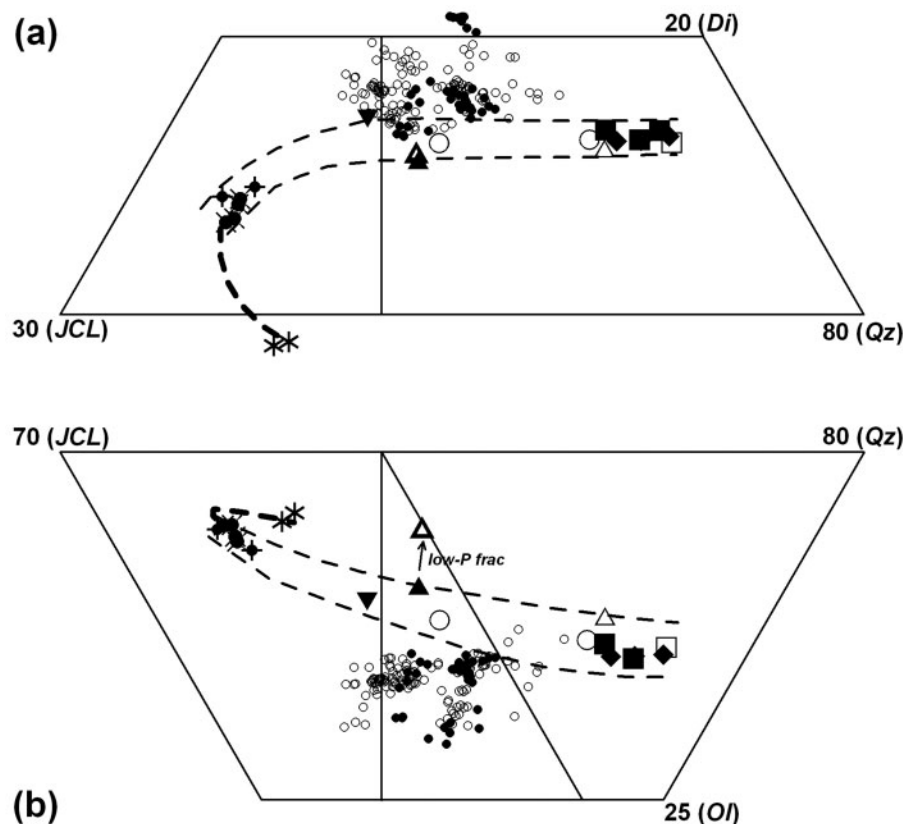


**Fig. 16.** Comparison of selected MORB glasses with liquid compositions in equilibrium with plagioclase lherzolite at 0.75 GPa. Based on the experimental liquid compositions, glasses were initially selected on the basis of  $\text{MgO} > 7 \text{ wt } \%$ ,  $\text{FeO} < 8 \text{ wt } \%$ . Glasses from the PETDB database ([www.petdb.org](http://www.petdb.org)) are plotted as small open circles. These glasses have  $61 < \text{Mg}\# < 69$ . Glasses from Danushevsky (2001), selected on the same criteria, are plotted as small filled circles and have  $62 < \text{Mg}\# < 69$ . These relatively primitive or parental glasses do not resemble melt compositions in equilibrium with plagioclase lherzolite at 0.75 GPa. The small arrow and open triangle in (b) shows the calculated low-pressure fractionation trend modeled by PETROLOG (Danushevsky, 2001) for olivine and plagioclase separation (see text).

### Harzburgite residues with sodic melts

In Fig. 15, there are three data points (small open circles) for melt compositions in equilibrium with spinel harzburgite residues; that is, plagioclase and clinopyroxene are absent. One of these (N64; Tables 2 and 3) is at the same temperature ( $1190^\circ\text{C}$ ) as the five-phase saturated melts of N62 and N63. The absence of both plagioclase and clinopyroxene is due to the much more sodic bulk composition. Similarly, at lower temperature ( $1160^\circ\text{C}$ ), layered experiments (L59, L60) have the assemblage of spinel harzburgite residues at a temperature within error of the  $\text{Ol} + \text{Opx} + \text{Plag} + \text{Sp} + \text{Liq}$  minimum melt of K99 and L43. The analyzed liquid of L59 lies on a trend from the minimum melt in the sodic system controlled by spinel harzburgite residue. Similarly, L60 and N64 experiments have the same bulk composition but are at temperatures  $\sim 30^\circ\text{C}$  apart. Both lie on the spinel harzburgite cotectic, along a vector towards orthopyroxene from a point on the  $\text{Ol} + \text{Opx} + \text{Plag} + \text{Sp} + \text{Liq}$  cotectic. As the bulk compositions are not calcium free, the orthopyroxenes have Ca

contents below that required for clinopyroxene saturation but reflecting the Ca contents of the coexisting melts.

### Plagioclase + spinel lherzolite residues and basaltic to 'trachytic' melts

The experimental data in complex 'natural' compositions demonstrate the compositional variance possible in basaltic compositions at 0.75 GPa. Liquids remain saturated by a five-phase ( $\text{Ol} + \text{Opx} + \text{Cpx} + \text{Plag} + \text{Sp}$ ) lherzolite mineralogy in which the mineral compositions are a close match with those of natural lherzolites.

The study brings together two approaches to the determination of lherzolite near-solidus melt compositions. The compositional shifts of melt compositions attributable to addition of components one by one to the CMAS system (the approach to complexity from a well-characterized simple system) can be discerned and at least partially resolved in the new data.

A consequence of this should be an improvement in empirical and thermodynamic modelling, as the data

characterize both melt compositions and mineral solid solutions. It demonstrates empirically the limitations that apply to mineral compositions because of coupled reactions among the coexisting phases. Thus referring to the data discussed and to Fig. 6 plotting  $An(Plag)$  vs  $Cr\#(spinel)$ , we infer that at 0.75 GPa, if the plagioclase is  $An_{80}$  to  $An_{95}$ , the limiting  $Cr\#$  of spinel on the plagioclase lherzolite solidus is approximately  $20 < Cr\# < 50$ . A more aluminous spinel ( $Cr\# < 20$ ) will react with pyroxenes to increase the anorthite content of plagioclase. A more Cr-rich spinel ( $Cr\# > 50$ ) will react with plagioclase, reducing its An content, to form aluminous spinel and pyroxenes. Considering natural lherzolites at 0.75 GPa, a spinel with  $Cr\# > 50$  will occur in the melting interval in two conditions: either the An content of plagioclase present is below  $An_{80}$ , or the plagioclase is eliminated and then melt is in equilibrium with  $Ol + Opx + Cpx + Sp$ . In that case, the alumina contents (and  $Cr\#$ ) of the pyroxenes track the spinel composition through coupled reactions involving  $NaCrSi_2O_6$ , Tschermak's silicate and Cr-Tschermak's silicate solid solutions in pyroxenes. At  $An_0$ , spinel does not become  $Cr_{100}$  because of coupled reactions with chromite and pyroxenes, as noted above.

If pressure is decreased, then we expect the limiting spinel compositions that can coexist with  $An_{80}$  plagioclase at the plagioclase lherzolite solidus to become more Cr-rich. If pressure is increased then the limiting spinel compositions on the plagioclase ( $An_{80}$ ) lherzolite solidus will become less Cr-rich.

It should be emphasized that cooling of a plagioclase lherzolite below the solidus at 0.75 GPa will also change the spinel, plagioclase and pyroxene solid solutions (Borghini *et al.*, 2010). The relations illustrated by our experiments are explicitly along the compositionally dependent solidus at 0.75 GPa.

## APPLICATION OF EXPERIMENTAL DATA TO THE PETROGENESIS OF MID-OCEAN RIDGE BASALTS

The rationale for our experimental study was summarized in the 'Introduction', including reference to models of mantle upwelling at low potential temperature and melt production near the 'cusp' on the fertile lherzolite solidus. In this section the compositions of liquids in equilibrium with a plagioclase + spinel lherzolite residue at 0.75 GPa are compared with compositions of analyzed glasses from mid-ocean ridge basalts (MORBs).

The experimental liquids are characteristically rich in silica and alumina with respect to the broad spectrum of natural basalts, and also are low in MgO and iron. These characteristics result in relatively high normative plagioclase and variations from quartz- and

hypersthene-normative to olivine- and hypersthene-normative as  $Ca/Na$  decreases in the five-phase-saturated liquids. The plagioclase phenocrysts of natural MORB are anorthite or bytownite and rarely labradorite (i.e.  $An_{95}$  to  $An_{60}$ ). Plagioclase in natural plagioclase lherzolites from ocean floor or ophiolite localities is also calcium-rich (Piccardo *et al.*, 2007, and references therein). Thus the experimental liquids in equilibrium with plagioclase  $> An_{60}$  and with  $Mg\# > 65$  (i.e. in equilibrium with olivine  $Mg\# > 85$ ) are the most relevant to compare with the natural basaltic glasses.

Noting the very large number of MORB glass analyses available in the PETDB database ([www.petdb.org](http://www.petdb.org)), the first step in seeking for matches with the experimental liquids was to select glasses with  $MgO > 7$  wt %,  $FeO < 8$  wt %; that is, approaching the  $Mg\#$  and low MgO contents of the experimental glasses. Only 118 analyses met these criteria from the ~16 500 analyses selected as 'All spreading centres', 'Glass', 'Electron Microprobe Analysis'. These natural glasses have  $61 < Mg\# < 69$ ; that is, they are slightly fractionated with respect to mantle residual olivine. Danushevsky (2001) has created a database of MORB glasses, including many selected as 'primitive' on the basis of the presence of magnesian olivine phenocrysts. He has obtained major element, trace element and water contents for the same glass sample. Although this database encompasses a much smaller sample set than PETDB, the selection is biased towards higher  $Mg\#$  glasses, and 38 of the 682 glasses have  $62 < Mg\# < 69$  (Danushevsky, 2001) and meet our preliminary screening criteria for 'matching' the experimental liquids. In both datasets (PETDB; Danushevsky, 2001), there is an inverse correlation between  $Na_2O$  and  $CaO$ , with  $Na_2O$  varying from 1.8 to 4.2 wt % and from 2.1 to 3.9 wt % in the two datasets respectively. At first inspection, there are similarities to the experimental liquids on the plagioclase + spinel lherzolite solidus at 0.75 GPa, where a similar range of  $Na_2O$  contents is characteristic for residual plagioclase from  $An_{80}$  to  $An_{65}$  from interpolation between our data points.

Plotting these 156 glass compositions in the normative tetrahedron (Fig. 16) shows a significant scatter. Most of the natural glasses do not overlie the five-phase-saturated liquids in either the projection from olivine or the projection from diopside. The more sodic compositions plot in the nepheline-normative field or close to the plane  $Ol-Cpx-Plag$ . This group of compositions has higher normative diopside [higher  $(Ca + Na)/Al$ ] and higher normative olivine than the liquids, which are in equilibrium with plagioclase + spinel lherzolite. In addition, the liquidus plagioclase of these liquids is more anorthitic than the plagioclase ( $\sim An_{55}$ ) of the experimental five-phase-saturated liquids near the plane  $Ol-Cpx-Plag$ . The more calcic of the 156 glass compositions also have higher

normative diopside contents than the experimental liquids and most have higher normative olivine contents. We have not identified any MORB glasses that have compositions complementary to a plagioclase lherzolite residue at 0.75 GPa, and in particular we have not identified liquids of magnesian quartz tholeiite character that match our experimental melts in equilibrium with plagioclase + spinel lherzolite with plagioclase of  $An_{80-95}$ .

In seeking evidence supporting the derivation of primitive MORB at low pressures, it is possible that lower pressure (magma chamber) separation of olivine + plagioclase, with plagioclase dominant in the accumulates, drives derivative liquids away from the plagioclase + spinel lherzolite (residue) position in the projection from olivine, and away from the plagioclase–olivine join in the projection from diopside. To test this hypothesis, we used the PETROLOG program (Danushevsky, 2001) applied to the N56 liquid composition. Olivine is the predicted liquidus phase at 1 atm pressure, joined by plagioclase after ~1% olivine crystallization and by clinopyroxene after ~5% olivine and ~15% plagioclase crystallization. The derivative liquids along this low-pressure fractionation trend diverge from the field of natural glasses towards lower normative olivine compositions (Fig. 16). This simple crystal fractionation hypothesis does not reconcile the compositions of the selected MOR glasses with the experimental 0.75 GPa liquids. A further argument against significant plagioclase fractionation in the most primitive MORB is the absence of any negative Eu anomaly (Chalot-Prat, 2005, and references therein). With respect to the objectives of this study, the experimentally determined liquid compositions that coexist with residual plagioclase + spinel lherzolites at 0.75 GPa are unlike any liquids yet identified among sampled glass compositions from mid-ocean ridge settings.

As the MORB glass compositions selected have  $61 < Mg\# < 69$  and thus are evolved with respect to equilibrium with mantle lherzolite, their relation to more primitive melts would need to be explored using evidence of phenocryst and melt inclusion compositions. This relationship could range from simple olivine precipitation from a more olivine-rich parent magma extracted from a plagioclase-free lherzolite residue at >1 GPa to models of crustal magma chamber processes with multiphase crystallization and successive magma chamber replenishment. The two hypotheses could be also combined. In any case, evidence in the mid-oceanic ridge environment for coupling between the eruptive process and mechanical extension parameters (Stakes *et al.*, 1984; Chalot-Prat, 2005) is indicative of the existence of shallow magma chambers and related structural and petrological interactions, and not of a shallow depth for the mid-ocean ridge mantle upwelling and magma segregation process.

In addition, referring to interpretations of mantle re-ferilization processes that produce natural plagioclase + spinel lherzolites by reactive porous flow into residual high-temperature lherzolite or harzburgite, the experimental data define the compositional path along which the hypothetical invasive basaltic or picritic liquid will evolve as an impregnated residue reacts, cools and progressively crystallizes in the uppermost mantle. End-products (plagioclase + spinel lherzolites) with plagioclase varying from anorthite to bytownite or labradorite may be investigated as possible magma–residue pairs using the experimental data in this study.

## CONCLUSIONS

An understanding of mantle melting and MORB petrogenesis builds upon detailed knowledge of not only liquid compositions but also liquidus phase compositions. Given sufficient experimental data encompassing the chemical complexity (six major and four minor oxide components) of natural rocks, experimental and thermodynamic approaches may be integrated to construct predictive models for the covariance of mineral and liquid phase compositions in  $P,T$  space. Our study is a contribution to this objective; that is, a detailed examination of the compositions of liquids at the solidus of plagioclase lherzolite at a pressure of 0.75 GPa (~27 km depth equivalent).

Liquids at the plagioclase + spinel lherzolite solidus are saturated in five phases (olivine, orthopyroxene, clinopyroxene, plagioclase and spinel), all of which are solid solutions in which major and minor components are determined by continuous reactions, including reactions with fictive components in the liquid. The data of Table 3 and binary plots of Figs 4–8 provide information that can be integrated with end-member, simple system data to yield general models of crystal–liquid equilibria.

The major solid solutions that control the liquid composition at the plagioclase + spinel lherzolite solidus are Na–Ca, Cr–Al and Fe–Mg. The Fe–Mg exchange is of limited petrogenetic significance as the mantle composition is inferred to be relatively constant at ~ $Mg_{90}$ . The experimental data show small effects of Fe–Mg variation, which are consistent with the direction and magnitude defined in the FCMAS system (Gudfinnsson & Presnall, 2000). The Cr–Al substitution in spinel and pyroxenes has an effect on liquid compositions, also consistent with the composition vector defined in the CrCMAS study (Liu & O'Neill, 2004). A larger effect is evident in the appearance of spinel as a solidus phase, owing to the addition of Cr to the CMAS, FCMAS or NCMAS systems at 0.75 GPa. Spinel is absent in these simple systems. Its appearance at the solidus produces a new cotectic (five-phase + Liq) at which the liquid composition for An-rich plagioclase is distinctly more siliceous and lower in normative olivine than the four-phase + Liq cotectic in CMAS (Fig. 12). This is a

significant modification to prediction of melt compositions from the end-member systems CMAS, FCMA, or NCMAS. Indeed, the change in liquid composition is a 'discontinuous' one, not predictable from the spinel-absent systems. A similar conclusion applies to the sodic end of the five-phase + Liq field, where the liquid at the four-phase + Liq (clinopyroxene-absent) cotectic is well removed from the limit (at An<sub>18</sub>) of the five-phase + Liq cotectic (Figs 11, 12 and 15). Within the compositional field of the five-phase + Liq cotectic, the Cr–Al range expressed in the spinel and coexisting pyroxenes compositions is limited by coupled reactions. The Cr–Al range becomes smaller and more Cr-rich as plagioclase becomes more sodic (Fig. 6b).

It is expected that in detailed comparisons of coexisting minerals in the experiments and in natural plagioclase lherzolite, the partitioning of Cr/Al and Na/Ca between spinel, plagioclase and pyroxene, and of Na/Ca between plagioclase and liquid will allow *P*/*T* determinations, in addition to existing Fe/Mg and pyroxene 'solvus' geothermometers. The integration of the data obtained in this study at the solidus with subsolidus mineral assemblages (e.g. Borghini *et al.*, 2010) should allow improved understanding of the conditions of crystallization of natural plagioclase lherzolites. The detailed mineral compositional data at the plagioclase lherzolite solidus will provide a useful template for comparison with natural plagioclase lherzolite, with a cursory examination showing that natural assemblages (if assumed to have crystallized at 0.75 GPa) must have crystallized at temperatures well below the solidus. Where this is the case, the use of minor or trace element abundances in pyroxenes to constrain hypothetical coexisting liquids is inappropriate without first restoring the subsolidus mineral assemblages to solidus conditions.

The experimental data demonstrate a major role for plagioclase composition in determining the composition of liquids in equilibrium with plagioclase lherzolite. Although there are small compositional shifts of five-phase-saturated liquids with Mg# variation and with Cr# of spinel, these are subordinate to the effects of plagioclase composition. At 0.75 GPa, as plagioclase varies from An<sub>95</sub> to An<sub>18</sub>, liquids vary from quartz-normative basalts, through olivine + hypersthene-normative basalts (basaltic andesites) to nepheline-normative 'trachytes' with 10 wt % Na<sub>2</sub>O, 60 wt % SiO<sub>2</sub> and 4 wt % MgO. Although examination of particular oxide concentrations, ratios or binary plots may be used for favourable comparison with natural MORB (e.g. high Al<sub>2</sub>O<sub>3</sub> and high CaO/Al<sub>2</sub>O<sub>3</sub>), the use of normative projections capturing the whole major element composition, and of key mineral and melt partitioning such as Mg# in olivine and pyroxenes and An (Ca#) content of plagioclase, demonstrates the differences between experimental liquids

equilibrated with plagioclase + spinel lherzolite and MORB glasses.

Particular attention is directed to liquid compositions equilibrated with plagioclase lherzolite at 0.75 GPa, ~1230°C, with plagioclase of An<sub>80</sub> to An<sub>95</sub> (i.e. similar to natural plagioclase lherzolites). These liquids do not match the compositions of natural MORB glasses and provide no support for hypotheses of separation of MORB from residual plagioclase lherzolite (i.e. with <10% melting of fertile lherzolite) at low pressure. We infer that any correlations between parental magma compositions and geodynamic parameters within the plate-tectonics paradigm are created at deeper levels and not at depths around 30 km.

## ACKNOWLEDGEMENTS

F.C.-P. thanks the Research School of Earth Sciences, and especially the Experimental Petrology group, for its warm welcome and the facilities (including strong financial and technical support) provided during her visits in 2005, 2006 and 2008. The technical support of David Clark, Bill Hibberson and Dean Scott of the Experimental Petrology group at the Research School of Earth Sciences, and of Dr Frank Brink of the Electron Microscope Unit of the Australian National University, is gratefully acknowledged. Professor H. St.C. O'Neill is thanked for discussions, support and access to the Experimental Petrology facilities at ANU. Constructive and detailed reviews by Giorgio Borghini, Shantanu Keshav and an anonymous reviewer were greatly appreciated. This is the CRPG-CNRS Contribution 2022.

## FUNDING

All authors acknowledge the support of the Australian Research Council in funding to DHG for research on upper mantle petrogenesis, and of the Petrochemistry and Experimental Petrology Group at Research School of Earth Sciences, The Australian National University, for laboratory maintenance, experimental costs and technical support, without which the project could not have been carried out. FCP acknowledges the support of the CRPG/CNRS for her travel expenses in 2005. DHG and TJF acknowledge funding support by School of Earth Sciences and Centre for Ore Deposits and Exploration Studies (CODES) at University of Tasmania.

## REFERENCES

- Ariskin, A. A. & Barmina, G. S. (1990). Equilibria thermometry between plagioclases and basalt or andesite magmas. *Geochemistry International* **27**(10), 129–134.
- Asimow, P. D., Hirschmann, M. M. & Stolper, E. M. (2001). Calculation of peridotite partial melting from thermodynamic models of minerals and melts; IV, Adiabatic decompression and

- the composition and mean properties of mid-ocean ridge basalts. *Journal of Petrology* **42**, 963–998.
- Borghini, G., Fumagalli, P. & Rampone, E. (2010). The stability of plagioclase in the upper mantle: subsolidus experiments on fertile and depleted lherzolite. *Journal of Petrology* **51**, 229–254.
- Chalot-Prat, F. (2005). An undeformed ophiolite in the Alps: field and geochemical evidences for a link between volcanism and shallow plate tectonic processes. In: Foulger, G. R., Natland, J. H., Presnall, D. C. & Anderson, D. L. (eds) *Plates, Plumes and Paradigms. Geological Society of America, Special Papers* **388**, 751–780.
- Danyushevsky, L. V. (2001). The effect of small amounts of H<sub>2</sub>O on crystallization of mid-ocean ridge and backarc basin magmas. *Journal of Volcanology and Geothermal Research* **110**, 265–280.
- Falloon, T. J., Green, D. H., O'Neill, H. S. C. & Hibberson, W. O. (1997). Experimental tests of low degree peridotite partial melt compositions, implications for the nature of anhydrous near-solidus peridotite melts at 1 GPa. *Earth and Planetary Science Letters* **152**, 149–162.
- Ford, C. E., Russell, D. G., Craven, J. A. & Fisk, M. R. (1983). Olivine–liquid equilibria: Temperature, pressure and composition dependence of the crystal/liquid cation partition coefficients for Mg, Fe<sup>2+</sup>, Ca and Mn. *Journal of Petrology* **24**, 256–265.
- Ghiorso, M. S., Hirschmann, M. M., Reiners, P. W. & Kress, V. (2002). The pMELTS; a revision of MELTS for improved calculation of phase relations and major element partitioning related to partial melting of the mantle to 3 GPa. *Geochemistry, Geophysics, Geosystems* **3**(5), 31–45.
- Green, D. H. & Falloon, T. J. (1998). Pyrolite: a Ringwood concept and its current expression. In: Jackson, I. N. S. (ed.) *The Earth's Mantle: Composition, Structure and Evolution*. Cambridge: Cambridge University Press, pp. 311–378.
- Gudfinnsson, G. H. & Presnall, D. C. (2000). Melting behavior of model lherzolite in the system CaO–MgO–Al<sub>2</sub>O<sub>3</sub>–SiO<sub>2</sub>–FeO at 0.7 to 2.8 GPa. *Journal of Petrology* **41**, 1241–1269.
- Hart, S. R. & Zindler, A. (1986). In search of a bulk-Earth composition. *Chemical Geology* **57**, 247–267.
- Herzberg, C. & O'Hara, M. J. (2002). Plume-associated ultramafic magmas of Phanerozoic age. *Journal of Petrology* **43**, 1857–1883.
- Jaques, A. L. & Green, D. H. (1980). Anhydrous melting of peridotite at 0–15 kb and the genesis of mid-ocean ridge basalts. *Contributions to Mineralogy and Petrology* **73**, 287–310.
- Liu, X. & O'Neill, H. (2004). The effect of Cr<sub>2</sub>O<sub>3</sub> on the partial melting of spinel lherzolite in the system CaO–MgO–Al<sub>2</sub>O<sub>3</sub>–SiO<sub>2</sub>–Cr<sub>2</sub>O<sub>3</sub> at 1.1 GPa. *Journal of Petrology* **45**, 2261–2286.
- McKenzie, D. P. & Bickle, M. J. (1988). The volume and composition of melt generated by extension of the lithosphere. *Journal of Petrology* **29**, 625–679.
- Müntener, O., Manatschal, G., Desmurs, L. & Pettke, T. (2010). Plagioclase peridotites in ocean–continent transitions: refertilized mantle domains generated by melt stagnation in the shallow mantle lithosphere. *Journal of Petrology* **51**, 255–294.
- Piccardo, G. B., Zanetti, A. & Müntener, O. (2007). Melt/peridotite interaction in the Southern Lanzo peridotite: Field, textural and geochemical evidence. *Lithos* **94**, 181–209.
- Presnall, D. C. & Hoover, J. D. (1987). High pressure phase equilibrium constraints on the origin of primary mid-ocean ridge basalts. In: Mysen, B. O. (ed.) *Magmatic Processes: Physico-chemical Principles. Geochemical Society, Special Publication* **1**, 75–89.
- Presnall, D. C., Dixon, J. R., O'Donnell, T. H. & Dixon, S. A. (1979). Generation of mid-ocean ridge tholeiites. *Journal of Petrology* **20**, 3–35.
- Presnall, D. C., Gudfinnsson, G. H. & Walter, M. J. (2002). Generation of mid-ocean ridge basalts at pressures from 1 to 7 GPa. *Geochimica et Cosmochimica Acta* **66**, 2073–2090.
- Spandler, C., Yaxley, G., Green, D. H. & Scott, D. (2010). Experimental phase and melting relations of metapelite in the upper mantle: implications for the petrogenesis of intraplate magmas. *Contributions to Mineralogy and Petrology* **160**, 569–589.
- Stakes, D. S., Shervais, J. W. & Hopson, C. A. (1984). The volcanic–tectonic cycle of the FAMOUS and AMAR valleys, Mid-Atlantic Ridge (36°47'N): evidence from basalt glass and phenocryst compositional variations for a steady state magma chamber beneath the valley midsections, AMAR 3. *Journal of Geophysical Research* **89**(B8), 6995–7028.
- Van Den Bleeken, G., Müntener, O. & Ulmer, P. (2010). Reaction processes between tholeiitic melt and residual peridotite in the uppermost mantle: an experimental study at 0.8 GPa. *Journal of Petrology* **51**, 153–183.
- Walter, M. J. & Presnall, D. C. (1994). Melting behavior of simplified lherzolite in the system CaO–MgO–Al<sub>2</sub>O<sub>3</sub>–SiO<sub>2</sub>–Na<sub>2</sub>O from 7 to 35 kbar. *Journal of Petrology* **35**, 329–359.